Re-evaluating ^{14}C dating accuracy in deep-sea sediment archives.

Bryan C. Lougheed

Department of Earth Sciences, Uppsala University, Sweden.

bryan.lougheed@geo.uu.se

(corresponding author)

Philippa Ascough

Scottish Universities Environmental Research Centre, Glasgow, Scotland, UK.

philippa.ascough@glasgow.ac.uk

Andrew M. Dolman

Alfred Wegener Institute, Helmholtz Centre for Polar and Marine Research, Potsdam, Germany

andrew.dolman@awi.de

Ludvig Löwemark

Department of Geosciences, National Taiwan University, Taipei, Taiwan.

ludvig@ntu.edu.tw

Brett Metcalfe

Department of Earth Sciences, Vrije Universiteit Amsterdam, the Netherlands.

LSCE-IPSL, CEA-CNRS-UVSQ, Université Paris-Saclay, Gif-sur-Yvette, France.

b.metcalfe@vu.nl

Re-evaluating ^{14}C dating accuracy in deep-sea sediment archives.

Bryan C. Lougheed[1], Philippa Ascough[2], Andrew M. Dolman[3], Ludvig Löwemark[4], Brett Metcalfe[5,6]

1. Department of Earth Sciences, Uppsala University, Sweden.
2. Scottish Universities Environmental Research Centre, Glasgow, Scotland, UK.
3. Alfred Wegener Institute, Helmholtz Centre for Polar and Marine Research, Potsdam, Germany
4. Department of Geosciences, National Taiwan University, Taipei, Taiwan.
5. Department of Earth Sciences, Vrije Universiteit Amsterdam, the Netherlands.
6. LSCE-IPSL, CEA-CNRS-UVSQ, Université Paris-Saclay, Gif-sur-Yvette, France

Corresponding author: B.C. Lougheed (bryan.lougheed@geo.uu.se)

Abstract

The current geochronological state-of-the-art for applying the radiocarbon (^{14}C) method to deep-sea sediment archives lacks key information on sediment bioturbation. Here, we apply a sediment accumulation model that simulates the sedimentation and bioturbation of millions of foraminifera, whereby realistic ^{14}C activities (i.e. from a ^{14}C calibration curve) are assigned to each single foraminifera based on its simulation timestep. We find that the normal distribution of ^{14}C age typically used to represent discrete-depth sediment intervals (based on the reported laboratory ^{14}C age and measurement error) is unlikely to be a faithful reflection of the actual ^{14}C age distribution for a specific depth interval. We also find that this deviation from the actual ^{14}C age distribution is greatly amplified during the calibration process. We find a systematic underestimation of total geochronological error in many cases (by up to thousands of years), as well as the generation of age-depth artefacts in downcore calibrated median age. Specifically, we find that even in the case of "perfect" simulated sediment archive scenarios, whereby sediment accumulation rate (SAR), bioturbation depth, reservoir age and species abundance are all kept constant, the ^{14}C dating and calibration process generates temporally dynamic median age-depth artefacts, on the order of hundreds of years – even in the case of high SAR scenarios of 40 cm ka^{-1} and 60 cm ka^{-1}. Such age-depth artefacts can be especially pronounced during periods corresponding to dynamic changes in the Earth's $\Delta^{14}C$, where single foraminifera of varying ^{14}C activity can be incorporated into single discrete-depth sediment intervals. In certain SAR scenarios, a discrete depth's true median age can consistently fall outside the 95.45% calibrated age range predicted by the ^{14}C dating and calibration process. Our findings suggest the possibility of ^{14}C-derived age-depth artefacts in the literature: since age-depth artefacts are likely to coincide with large-scale changes in global $\Delta^{14}C$, which themselves can coincide with large-scale changes in global climate (such as the last deglaciation), ^{14}C-derived age-depth artefacts may have been previously been (partially) misinterpreted as due to changes in

global climate. Our study highlights the need for the development of improved deep-sea sediment ^{14}C calibration techniques that include an *a priori* representation of bioturbation for multi-specimen samples.

1.0 Introduction

For over half a century, radiocarbon (^{14}C) dating has been applied to deep sea sediment archives. The material that is typically analysed from these archives consists of the calcareous tests of foraminifera. The minimum amount of material required for viable ^{14}C analysis has meant that researchers have had to pick tens to hundreds of individual foraminifera specimens (depending on specimen size) from a single discrete-depth core interval (typically 1 cm of core depth) and combine these into a single subsample for analysis. Such multi-specimen samples are likely to be heterogeneous in ^{14}C age (i.e. combine individual specimens of varying true age). The ^{14}C laboratory measurement (and reported machine error) applied to such an amalgamated multi-specimen sample will simply represent the mean ^{14}C activity of the total carbon of all individual specimens. Consequently, the true intra-sample ^{14}C age heterogeneity of a sample is concealed from the researcher. Failure to consider the actual ^{14}C age heterogeneity of multi-specimen samples can lead to downcore ^{14}C age artefacts when post-depositional processes mix foraminifera with differing ^{14}C activities, especially during periods coinciding with periods of dynamic $\Delta^{14}C$ history of the Earth. Furthermore, one must also take into consideration that younger specimens within a subsample contribute exponentially more to the subsample's mean ^{14}C activity than older specimens do, a process referred to as the isotope mass balance effect (Erlenkeuser, 1980; Keigwin and Guilderson, 2009), due to ^{14}C being a radioactive isotope (specimen ^{14}C activity decreases exponentially with the passing of time).

Systematic bioturbation has long been recognised as an inherent feature of deep-sea sediment archives (Bramlette and Bradley, 1942; Arrhenius, 1961; Olausson, 1961). Long-established mathematical models of bioturbation in deep-sea sediment archives consider the uppermost ~10 cm of a sediment archive to be uniformly mixed due to active bioturbation - the bioturbation depth (BD) (Berger and Heath, 1968; Berger and Johnson, 1978; Berger and Killingley, 1982). The presence of such a BD has been supported by the detection of a uniform mean age in the uppermost intervals of sediment archives (Peng et al., 1979; Trauth et al., 1997; Boudreau, 1998; Teal et al., 2008) and by the ^{14}C analysis of single foraminifera (Lougheed et al., 2018). The total range of single specimen ages mixed within the BD is dependent upon two main factors: the depth of the BD itself, and the sediment accumulation rate (SAR), both of which can exhibit spatiotemporal variation due to environmental and biological factors (Müller and Suess, 1979; Trauth et al., 1997). The presence of uniform mixing within the BD throughout the sedimentation history of a deep-sea sediment archive ultimately results, in the case of temporally constant SAR and BD, in the single specimen population of discrete sediment intervals being characterised by an exponential probability density function (PDF) for true age, with a maximum probability for younger ages and a long tail towards older ages. The existence of such a distribution has been supported by the post-depositional mixing of tephra layers (Bramlette and Bradley, 1942; Nayudu, 1964; Ruddiman and Glover, 1972; Abbott et al., 2018) and the smoothing out of the downcore mean signal (Guinasso and Schink, 1975; Pisias, 1983; Schiffelbein, 1984; Bard et al., 1987; Löwemark et al., 2008; Trauth, 2013), the smoothing of which can change downcore in tandem with foraminiferal abundance changes (Ruddiman et al., 1980; Peng and Broecker, 1984; Paull et al., 1991; Löwemark et al., 2008). If SAR, BD and the $\Delta^{14}C$ history of the Earth were all to be temporally constant, then the idealised ^{14}C activity PDF of each discrete depth (expressed as, e.g., the $^{14}C/^{12}C$ ratio or fraction modern [$F^{14}C$]) would, therefore, exhibit the combination of two exponential functions (the exponential PDF of true age plus the exponential PDF of ^{14}C activity vs time predicted by the half-life of ^{14}C). However, the distribution of the ^{14}C activity PDF is made complicated by the fact that ^{14}C activity vs time is not always the exact exponential function that would be predicted by the radioactive half-life of ^{14}C, seeing as the Earth exhibits a dynamic $\Delta^{14}C$ history with temporal changes in atmospheric ^{14}C activity (Suess, 1955, 1965; de Vries, 1958). These changes are brought about by changes in ^{14}C production in the atmosphere in combination with climatic and oceanic influence upon the carbon cycle (Craig, 1957; Damon et al., 1978; Siegenthaler et al., 1980). Furthermore, non-uniform mixing of the oceans can contribute to temporal changes in local water ^{14}C activity at a given coring site.

When applying the ^{14}C method to sediment core material, researchers represent the ^{14}C age of a discrete-depth interval using a normal (Gaussian) distribution, based on the conventional mean ^{14}C age and measurement error reported by the ^{14}C laboratory (Stuiver and Polach, 1977). In some cases, this ^{14}C age normal distribution is widened by researchers to incorporate a reservoir age uncertainty, but it remains a normal distribution. This normal distribution of ^{14}C age is subsequently calibrated using a suitable reference record of past $\Delta^{14}C$ (e.g. those produced by the *IntCal* group), allowing researchers to arrive at an estimation of the discrete depth interval's true (i.e. calendar) age. Such an approach inherently excludes the effects of bioturbation, because one would not expect a normal ^{14}C age distribution to be representative of a discrete depth interval, for the reasons described in the previous paragraph. Currently, systematic investigation is lacking into whether neglecting to include the effects of bioturbation has significant impact upon the interpretative accuracy of ^{14}C dating as it is currently applied in palaeoceanography, i.e. if it may ultimately lead to spurious downcore geochronological interpretations or not. To investigate for the presence of such artefacts, we employed the $\Delta^{14}C$-enabled, single-specimen SEdiment AccuMUlation Simulator (SEAMUS) (Lougheed, 2019). This model uses a similar understanding of bioturbation as included in existing bioturbation models (Trauth, 2013; Dolman and Laepple, 2018), but differs in that it explicitly simulates the accumulation and bioturbation of single foraminifera, each with individually assigned ^{14}C activities, to create a synthetic sediment archive history. Subsequently, current palaeoceanographic subsampling and ^{14}C dating practices are virtually applied to the 1 cm discrete depths of the model's outputted synthetic archive, resulting in discrete-depth ^{14}C ages and calibrated ages that are representative of the existing palaeoceanographic state-of-the-art. These results are subsequently compared to the actual discrete-depth ^{14}C-calibrated age and true age distributions predicted by the model, allowing us to quantitatively evaluate contemporary palaeoceanographic ^{14}C dating and calibration techniques.

2.0 Method

2.1 The synthetic core simulation

The SEAMUS model (Lougheed, 2019) synthesises *n* number of single foraminifera raining down from the water column per simulation timestep, whereby *n* is the capacity of the synthetic sediment archive being simulated (analogous to core radius) scaled to the SAR of the timestep as predicted by an inputted age-depth relationship (Lougheed, 2019). To provide good statistics, all simulations use a timestep of 5 years and 10^4 synthetic foraminifera per cm core depth. An abundance of 10^4 specimens per cm is also similar to a best-case scenario value for a particular subsample in the field (Broecker et al., 1992). In each timestep, all newly created single foraminifera are assigned an age (corresponding to the timestep), a sediment depth (according to the age-depth input), as well as a ^{14}C age (in ^{14}C yr BP) and normalised ^{14}C activity (in $F^{14}C$) based on *Marine13* (Reimer et al., 2013) after the application of a prescribed reservoir age for the timestep. For older sections of the *Marine13* calibration curve, where only 10 year timesteps are available, linear interpolation is used to provide a 5 year ^{14}C activity timestep resolution. The simulation uses a synthetic ^{14}C blank value corresponding to the lowest activity value in *Marine13* (46806 ^{14}C yr BP), i.e. any single foraminifera that are too old to be assigned a ^{14}C activity using *Marine13* are simply assigned a ^{14}C activity (in $F^{14}C$) corresponding to 46806 ^{14}C yr BP. As we are simulating a core with synthetic foraminifera and synthetic ^{14}C dates, we can essentially choose any blank value we desire, and the oldest value within *Marine13* is therefore appropriate. It is also a useful blank value because, in practice, it is not possible to correctly calibrate samples containing single specimens with ^{14}C ages older than those contained within the calibration curve. After the creation of all new single foraminifera within the synthetic core for a specific timestep, bioturbation is simulated. Specifically, for each timestep the depth values corresponding to all simulated foraminifera within the contemporaneous BD are each assigned a new depth by way of random sampling of the BD interval. In this way, uniform mixing of foraminifera within the BD is simulated following established understanding of bioturbation (Berger and Heath, 1968; Trauth, 2013). All of the aforementioned processes are repeated for every simulation timestep until such point that the end of the age-depth input (i.e. the final core top) is reached. All simulations are initiated at 70 ka (in true age) in order to confidently exclude the influence of model spin-up effects upon our period of interest (0 – 45 ka), given the possibility of a given cm of sediment to have a long-tail (up to 20 ka, dependent on the scenario) of older foraminifera specimens. While SEAMUS can in principle be run on a local machine, to save time multiple simulations were run in parallel on a computing cluster provided by the Swedish National Infrastructure for Computing (SNIC) at the Uppsala Multidisciplinary Centre for Advanced Computational Science (UPPMAX).

2.2 Virtual discrete-depth analysis

After the completion of the synthetic core simulation, synthetic foraminifera (and corresponding values for true age, $F^{14}C$, and ^{14}C age) are picked from each discrete 1 cm interval of the sediment core. Subsequently, each of these picked 1 cm subsamples also undergoes a synthetic ^{14}C determination analogous to a perfect accelerator mass spectrometry (AMS) measurement, whereby the mean ^{14}C activity (in $F^{14}C$) for the entire subsample is calculated by taking the mean of all $F^{14}C$ values of all the single foraminifera within the picked subsample. Using the Libby half-life, this mean $F^{14}C$ value is also reported as a conventional ^{14}C age determination (in ^{14}C yr). All such synthetic determinations are assigned a synthetic 1σ measurement error analogous to a typical laboratory-reported counting error for a large sample. The prescribed synthetic measurement error ranges from 30 ^{14}C yr in the case of near-modern samples to 200 ^{14}C yr in the case of samples nearing the blank value, and are linearly scaled to $F^{14}C$, such that the error increases exponentially with ^{14}C age. Synthetic laboratory ^{14}C determinations and associated synthetic measurement uncertainties for each 1 cm slice are subsequently converted to calibrated years within SEAMUS using the embedded MatCal (v 2.5) ^{14}C calibration software (Lougheed and Obrochta, 2016), the Marine13 calibration curve (Reimer et al., 2013) and a prescribed reservoir age (according to the scenario – see following sections), to produce a calibrated age probability density function (PDF) for every cm core depth, i.e. analogous to what would be typically produced using contemporary palaeoceanography methods in the case of every discrete cm of core depth being ^{14}C dated.

3.0 Best case scenario simulations

In order to investigate the baseline accuracy when applying ^{14}C dating to deep-sea sediment cores, the first simulations in this study consider a number of ‘best case scenarios’ under perfect conditions. Essentially, we seek to test how well the current application of ^{14}C within palaeoceanography would function in the case of a theoretical perfect sediment core at a location with perfect water conditions. In these ‘perfect’ simulations, we therefore assume that *Marine13* constitutes a perfect reconstruction of past surface-water ^{14}C activity at the synthetic core site, and we therefore employ a temporally constant reservoir age ($\Delta R = 0$ ^{14}C yr). Furthermore, we assume a scenario involving synthetic sediment cores with temporally constant SAR and BD, and we also assume that the synthetic core is made up of a single planktonic foraminiferal species with a temporally constant abundance (10^4 cm^{-1}) and specimen size. A total of five best case scenarios are carried out, with five different SAR scenarios (5, 10, 20, 40 and 60 cm ka^{-1}). The BD is set to 10 cm in all cases, following established understanding of global BD (Trauth et al., 1997; Boudreau, 1998). In this scenario, we also assume perfection in sub-sampling, in that it that it is possible to exhaustively subsample all foraminifera material from each 1 cm discrete-depth interval when picking for multi-specimen samples. The results of these five scenarios are visualised in Fig. 1 and Fig. S1-S5.

A second set of best-case scenarios takes into account that older foraminifera have accumulated a longer residence time in the active bioturbation depth. These foraminifera are more likely to be broken and/or dissolved (Rubin and Suess, 1955; Ericson et al., 1956; Emiliani and Milliman, 1966; Barker et al., 2007), and are thus less likely to be picked by palaeoceanographers who preferentially pick whole/unbroken foraminifera specimens for analysis. In this way palaeoceanographers may exclude the oldest, least-well preserved fraction of the sediment. An indication of the BD residence time of single specimens for a given 1 cm discrete depth is shown in Fig. 2 for all five simulated SAR scenarios, along with the median and 90th percentile residence time. The percentage of broken specimens within the sediment archive is chiefly governed by the aforementioned BD residence time, bottom water chemistry (Bramlette, 1961; Berger, 1970; Parker and Berger, 1971), and the susceptibility of a particular foraminifera species to dissolution/breakage (Ruddiman and Heezen, 1967; Boltovskoy, 1991; Boltovskoy and Totah, 1992). Previous studies have indicated that foraminifera test breakage for typically analysed species at locations above the lysocline can hover around 10% (Le and Shackleton, 1992). In the second set of best-case scenarios we, therefore, exclude from the picking process for each 1 cm discrete depth all foraminifera with a number of bioturbation cycles greater than the 90th percentile for that particular discrete depth. This broken foraminifera percentage of 10% is applied to all five SAR scenarios (5, 10, 20, 40, 60 cm ka^{-1}) in a second set of best case scenarios, shown in Fig. 3 and Fig. S6-S10. One should be aware, however, that BD residence time is likely directly related to SAR itself: when sediment accumulation is slower, single specimens remain in the BD for relatively longer than in the case of faster SAR (Bramlette, 1961).

3.1 ^{14}C age artefacts

Radiocarbon analysis focuses on determining the mean ^{14}C activity of a particular sample, which is reported together with an associated analytical error. This mean activity is often reported by the laboratory as conventional ^{14}C age in ^{14}C yr BP. ^{14}C age is linear vs time, whereas ^{14}C activity is exponential vs time, due to ^{14}C being a radioactive isotope. Therefore, with increasing age heterogeneity of a sample, we can expect that the offset between the laboratory reported AMS conventional ^{14}C age of a sample to diverge from the idealised mean ^{14}C age of all single specimens within the sample. In Fig. 1, we compare the simulated AMS mean ^{14}C age calculated for each discrete depth to the idealised mean ^{14}C age (based on the mean value of all single foraminifera ^{14}C ages contained within a subsample). The resulting offset can help shed light upon how the measurement of age-heteregenous material is inherently biased towards younger (higher ^{14}C activity) specimens contained within the sample. We find that the AMS mean ^{14}C age is generally younger than the idealised mean ^{14}C age in all cases. This effect can be attributed to the fact that younger foraminifera within a heterogeneous subsample contribute exponentially more to a subsample's mean ^{14}C activity (what the measurement process is actually analysing) than older foraminifera do. This bias towards younger foraminifera is much most apparent in cases with large intra-sample heterogeneity, such as in scenarios with lower SAR (Fig. 1a), and is also reduced somewhat in the case of more broken foraminifera (Fig. 3a), resulting in lesser older foraminifera being picked, thus reducing the age heterogeneity. In the case of the highest SAR scenarios (> 40 cm ka^{-1}) the aforementioned bias is insignificant in a practical sense, in that it falls within the typical ^{14}C measurement error. For all scenarios, superimposed upon the general bias are artefacts of the Earth's dynamic $\Delta^{14}C$ history, caused by foraminifera from times of markedly differing $\Delta^{14}C$ to be mixed together into a single subsample, thus altering a subsample's ^{14}C activity distribution and causing downcore dynamic offsets between AMS mean ^{14}C age and idealisedmean ^{14}C age. The most pronounced example of these artefacts can be seen during known periods of dynamic $\Delta^{14}C$, such as during the Laschamps geomagnetic event (ca. 40~41 ka) (Guillou et al., 2004; Laj et al., 2014), when a large spike in atmospheric ^{14}C production occurred (Muscheler et al., 2014). We note that our simulations assign single foraminifera ^{14}C activity using the *Marine13* calibration curve, while newer records of $\Delta^{14}C$ (Cheng et al., 2018) suggest that the Laschamps $\Delta^{14}C$ excursion may have been of greater magnitude than was previously thought. A larger excursion would generate even more pronounced ^{14}C artefacts in the downcore, multi-specimen, discrete-depth record. Furthermore, there may exist of as yet undiscovered, past short-lived excursions in $\Delta^{14}C$ (Miyake et al., 2012, 2017; Mekhaldi et al., 2015).

We can also visualise how well a sample's ^{14}C probability distribution function (PDF) is represented by a ^{14}C age normal distribution based on AMS mean ^{14}C age and 1σ measurement error. This visualisation is shown on the vertical axes of Fig. 1d-i and Fig. 2d-i for a number of simulated discrete depths for the different SAR scenarios with a BD of 10 cm. It can be clearly seen that that the normal distribution derived from a subsample's AMS mean ^{14}C age and measurement uncertainty is a poor representation of a subsample's actual ^{14}C age distribution. In no cases, neither for high nor low SAR, does it correctly represent the true shape of the ^{14}C age distribution.

3.2 Calibration amplifies ^{14}C age distribution mischaracterisation

When estimating a true age distribution for a particular sample, researchers calibrate a normal distribution of ^{14}C age using suitable calibration curve (in this case *Marine13*). As discussed in the previous section, the aforementioned normal distribution of ^{14}C derived from the measurement mean and machine error is not a faithful representation of the actual ^{14}C age distribution for a particular discrete depth. Such a misrepresentation has the potential to be further amplified during the calibration process itself, potentially resulting in a poor estimation of a discrete depth's 95.45% age range and/or median age, the latter of which is often used to calculate e.g. sedimentation rates, or represents the region of highest probability which will steer age-depth modelling routines. In Fig. 1b (0% broken foraminifera) and Fig. 3b (10% broken foraminifera), we show the offset between each discrete depth's true median age, and the corresponding median age derived from ^{14}C calibration process. We find large offsets for all constant SAR scenarios, ranging from ~200 years in the case of the the 60 cm ka^{-1} scenario, to up to ~700 years in the case of the 5 cm ka^{-1} scenario. In certain scenarios, the true median age can consistently fall outside the 95.45% age range predicted by the ^{14}C dating and calibration process. A ~95% certainty suggests that, statistically, the true median will fall outside of the calibrated age range in only ~5% of cases, but in the case of the 5 cm ka^{-1} scenario (Fig. S1), the true median falls outside of the 95.45% calibrated age range for 43% of the discrete depths spanning the 0 – 40 cal ka period. In the case of 10% broken foraminifera, the offsets are reduced slightly in the case of the lower SAR scenarios.

All offsets for all scenarios vary dynamically downcore, meaning that they can potentially cause spurious interpretations of changes in SAR. Furthermore, as these offsets occur during periods of dynamic $\Delta^{14}C$, which can be caused by large-scale changes in the carbon cycle caused by climate shifts (such as during the last deglaciation), it is possible that some apparent changes in SAR in the palaeoceangraphic literature may have been erroneously attributed to climate processes, when they may be (partially) an artefact of the current application of ^{14}C dating and calibration within palaeoceanography.

Using the simulation output, it is also possible to quantitatively estimate how well the current ^{14}C dating and calibration state-of-the-art applied within palaeoceanography estimates the true age range contained within discrete-depth sediment intervals. The offset between the calibrated 95.45% age range and the true 95.45% age range for each discrete depth for all SAR scenarios is shown in Fig. 1c (0% broken foraminifera) and Fig. 3c (10% broken foraminifera) and is further visualised for all scenarios in Fig. S1-S10. For the lower SAR scenarios, the current application of ^{14}C dating within palaeoceanography significantly underestimates the total age range contained within each discrete-depth, by many thousands of years. The underestimation is less in the case of the scenario with 10% broken foraminifera. In the case of higher SAR scenarios, the discrete-depth 95.45% age range predicted by the ^{14}C calibration process is similar to that of the discrete depth 95.45% age range of the sediment itself. In some cases with very high SAR, the ^{14}C calibration process actually overestimates the 95.45% age range (e.g. Fig. 1e, Fig. 3e, Fig. S5 and Fig. S10).

3.3 The influence of ^{14}C-dead foraminifera

A general consequence of bioturbation and the subsequent mixing of single foraminifera specimens is that older foraminifera become systematically mixed upwards throughout the sedimentation history of a sediment archive. This general mixing can have a particular consequence near the analytical limit the ^{14}C method, in that foraminifera with a ^{14}C age that is beyond the analytical sensitivity can become mixed into samples. ^{14}C determinations with a ^{14}C age that is older than the established ^{14}C blank value (i.e. the sensitivity of the analytical process) are referred to as "^{14}C-dead". Within older intervals of heterogeneous deep-sea sediment archives, it is possible that a multi-specimen sample with an apparent measured ^{14}C age that is younger than the ^{14}C blank value can contain a significant proportion of ^{14}C-dead foraminifera. The presence of these ^{14}C-dead specimens within a sample will bias the sample's apparent measured ^{14}C age towards a too young value. Such artefactually young ^{14}C ages could ultimately erroneously be interpreted as age-depth features. In Table 1, the very first downcore occurrence of at least one simulated ^{14}C-dead foraminifer is detailed for each of the aforementioned constant SAR scenarios introduced in Section 3.0. In the case of low SAR scenarios with 0% broken foraminifera, ^{14}C-dead foraminifera are already present in discrete-depth samples with apparent AMS ages that would normally be considered well above the ^{14}C blank value, e.g. an apparent AMS age of 22647 ^{14}C yr BP in the case of 5 cm ka^{-1}, and 33747 ^{14}C yr BP in the case of 10 cm ka^{-1}. However, the contribution of ^{14}C-dead foraminifera at these levels may still be insignificant. The exact percentage contribution of ^{14}C-dead foraminifera to discrete depth AMS determinations is, therefore, detailed in Fig. 4a, 4c, 4e, 4g and 4i. From this analysis, it transpires that the first occurrence4 of at least 1% contribution of ^{14}C-dead foraminifera to discrete-depth AMS determinations occurs in the case of AMS ages of 39158 ^{14}C yr BP and 43601 ^{14}C yr BP, respectively for the 5 cm ka^{-1} and 10 cm ka^{-1} scenarios.

In the case of scenarios involving 10% broken foraminifera, older foraminifera within discrete-depth sediment intervals are no longer whole, and therefore not picked for subsamples by a palaeoceanographer preferring whole specimens. The consequence of this effect is the first occurrence of picked ^{14}C-dead whole foraminifera occurs much further downcore (Table 2, Fig. 4b, 4d, 4f, 4h and 4j). This finding further underlines the importance of understanding foraminifera preservation conditions for particular species and/or water chemistry, and the associated consequences for ^{14}C dating. As detailed in the method section, we have set the ^{14}C blank value at 46806 ^{14}C yr BP within the model simulation. The laboratory blank value in most laboratories is around ~50000 ^{14}C yr BP, or older, depending on sample size and preparation conditions. For such a blank value, essentially the same functions as shown in Fig. 4 would apply (assuming there are no as of yet undiscovered, large $\Delta^{14}C$ excursions around the period of the blank age), but shifted further to the right on the x-axis (such that the 100% ^{14}C-dead contribution exactly coincides with 50000 ^{14}C yr BP).

4.0 Dynamic sediment core scenario

The multiple sediment archive scenarios carried out in Section 3.0 all involved "perfect" input conditions with constant SAR. In Fig. 5, a scenario with dynamic inputs (Fig. 5a-d) for SAR and species abundance is considered. In this scenario, a sudden reduction in SAR (from 10 cm ka^{-1} to 5 cm ka^{-1}) and species abundance (from 50% abundance to 25% abundance) is inserted into the simulation at 11 ka. Reservoir age (ΔR) and BD are both kept constant, and a constant percentage of broken foraminifera of 10% is applied. The main consequence of such dynamic input is that, unlike the scenarios with constant input, the distribution for true age is no longer always a perfect exponential function (e.g. Fig. 5i and 5j). Specifically, changes in abundance and SAR can cause multi-modal true age population distributions for particular downcore discrete depths, which are not well captured by the calibrated age distribution resulting from the ^{14}C dating and calibration process (Fig. 5j). Furthermore, dynamic offsets between the true median age and calibrated median age occur around or near the change in SAR and abundance at 11 ka (Fig. 5f), meaning that the resulting ^{14}C-derived calibrated age-depth relationship doesn't correctly track the true age-depth relationship of the sediment archive simulation (Fig. S11). Finally, as is expected for a relatively low SAR scenario, the current palaeoceanographic geochronological state-of-the-art systematically underestimates the true age range of the sediment archive, with the underestimation being greater during the 5 cm ka^{-1} section of sediment archive than the 10 cm ka^{-1} section (Fig. 5f and S11).

5.0 Conclusion

This study demonstrates the possibility for the current ^{14}C dating and calibration method, as it is applied to multi-specimen samples within palaeoceanography, to produce age-depth artefacts, even in the case of theoretically perfect sediment archives where SAR, BD, species abundance and reservoir age are all constant. We also find that high SAR sediment archives (40 cm/ka^{-1} and 60 cm/ka^{-1}) are not immune to the generation of age-depth artefacts. Additional age-depth artefacts can be generated in the case of real-world sediment archives where the aforementioned SAR, BD, species abundance and reservoir age processes are inherently dynamic. Researchers should be aware, therefore, of the possible existence of such artefacts when interpreting deep-sea sediment geochronologies developed using ^{14}C methods applied to multi-specimen samples. Key to understanding the possible existence of such artefacts is a good quantification of the possible magnitude of temporal change in both foraminiferal abundance and preservation conditions. It may also be necessary to revisit existing studies and re-evaluate the magnitude of changes in deep-sea sediment SAR inferred from ^{14}C-based geochronologies, especially close to periods of dynamic $\Delta^{14}C$ and/or foraminiferal abundance. We note that even $\delta^{18}O$-based geochronologies (e.g., those developed using orbital tuning) are affected by temporal changes in foraminiferal abundance (Bard, 2001; Löwemark and Grootes, 2004; Löwemark et al., 2008).

6.0 Outlook

We propose that the ^{14}C calibration process for deep-sea sediment archives could be improved to include bioturbation *a priori*, seeing that no information regarding bioturbation is included in the current palaeoceanographic state-of-the-art with regards to ^{14}C dating. This new approach would involve constructing a representative distribution for ^{14}C age that includes *a priori* information regarding the approximate SAR and BD of the sediment archive, while also taking into account some basic information regarding possible changes in species abundance. Such a process would go some way to providing more realistic uncertainties (i.e. 95.45% age range) to ^{14}C-derived age-depth geochronologies in deep-sea sediment archives.

Finally, we note that increased automation and cost-effectiveness in ^{14}C analysis of ultra-small carbonate samples (Ruff et al., 2010; Lougheed et al., 2012; Wacker et al., 2013b, 2013a) can allow for the parallel measurement of $\delta^{18}O$, $\delta^{13}O$ and ^{14}C on a single foraminifer of suitable size (Lougheed et al., 2018), thereby allowing for the extraction of both age and palaeoclimate data from single foraminifer in a manner that is independent of the depth aspect of deep-sea sediment archives.

Author contributions

BCL carried out the model runs, with scenarios conceived with input from BM. BCL wrote the manuscript with input from the co-authors.

Acknowledgements

This work was funded by Swedish Research Council (Vetenskapsrådet – VR) Starting Grant number 2018-04992 awarded to BCL. The Swedish National Infrastructure for Computing (SNIC) at the Uppsala Multidisciplinary Centre for Advanced Computational Science (UPPMAX) provided computing resources. BM is supported by a Laboratoire d'excellence (LabEx) of the Institut Pierre-Simon Laplace (Labex L-IPSL), funded by the French Agence Nationale de la Recherche (grant no. ANR-10-LABX-0018). LL acknowledges support from Ministry of Science and Technology (06-2116-M-002-021 to LL), and the Featured Areas Research Center Program within the framework of the Higher Education Sprout Project by the Ministry of Education (MOE) of Taiwan.

References

Abbott, P. M., Griggs, A. J., Bourne, A. J. and Davies, S. M.: Tracing marine cryptotephras in the North Atlantic during the last glacial period: Protocols for identification, characterisation and evaluating depositional controls, Marine Geology, 401, 81–97, doi:10.1016/j.margeo.2018.04.008, 2018.

Arrhenius, G.: Geological record on the ocean floor, in Oceanography, pp. 129–148, Am. Assoc. Advan. Sci Washington, DC., 1961.

Bard, E.: Paleoceanographic implications of the difference in deep□sea sediment mixing between large and fine particles, Paleoceanography, 16(3), 235–239, 2001.

Bard, E., Arnold, M., Duprat, J., Moyes, J. and Duplessy, J. C.: Reconstruction of the last deglaciation: Deconvolved records of δ 18 O profiles, micropaleontological variations and accelerator mass spectrometric 14 C dating, Climate Dynamics, 1(2), 101–112, 1987.

Barker, S., Broecker, W., Clark, E. and Hajdas, I.: Radiocarbon age offsets of foraminifera resulting from differential dissolution and fragmentation within the sedimentary bioturbated zone, Paleoceanography, 22(2), doi:10.1029/2006PA001354, 2007.

Berger, W. H.: Planktonic foraminifera: selective solution and the lysocline, Marine Geology, 8(2), 111–138, 1970.

Berger, W. H. and Heath, G. R.: Vertical mixing in pelagic sediments, Journal of Marine Research, 26, 134–143, 1968.

Berger, W. H. and Johnson, R. F.: On the thickness and the 14C age of the mixed layer in deep-sea carbonates, Earth and Planetary Science Letters, 41(2), 223–227, 1978.

Berger, W. H. and Killingley, J. S.: Box cores from the equatorial Pacific: 14C sedimentation rates and benthic mixing, Marine Geology, 45(1), 93–125, doi:10.1016/0025-3227(82)90182-7, 1982.

Boltovskoy, E.: On the destruction of foraminiferal tests (laboratory experiments), Révue de Micropaléontologie, 34(1), p12-25, 1991.

Boltovskoy, E. and Totah, V.: Preservation index and preservation potential of some foraminiferal species, Journal of Foraminiferal Research, 22(3), 267–273, doi:10.2113/gsjfr.22.3.267, 1992.

Boudreau, B. P.: Mean mixed depth of sediments: The wherefore and the why, Limnology and Oceanography, 43(3), 524–526, doi:10.4319/lo.1998.43.3.0524, 1998.

Bramlette, M. and Bradley, W.: Geology and biology of North Atlantic deep-sea cores. Part 1. Lithology and geologic interpretations, Prof. Pap. U.S. Geol. Surv., 196 A, 1–34, 1942.

Bramlette, M. N.: Pelagic sediments., Oceanography, 345–366, 1961.

Broecker, W., Bond, G., Klas, M., Clark, E. and McManus, J.: Origin of the northern Atlantic's Heinrich events, Climate Dynamics, 6(3), 265–273, doi:10.1007/BF00193540, 1992.

Cheng, H., Edwards, R. L., Southon, J., Matsumoto, K., Feinberg, J. M., Sinha, A., Zhou, W., Li, H., Li, X., Xu, Y., Chen, S., Tan, M., Wang, Q., Wang, Y. and Ning, Y.: Atmospheric 14C/12C changes during the last glacial period from Hulu Cave, , 6, 2018.

Craig, H.: The Natural Distribution of Radiocarbon and the Exchange Time of Carbon Dioxide Between Atmosphere and Sea, Tellus, 9(1), 1–17, doi:10.1111/j.2153-3490.1957.tb01848.x, 1957.

Damon, P. E., Lerman, J. C. and Long, A.: Temporal Fluctuations of Atmospheric 14C: Causal Factors and Implications, Annu. Rev. Earth Planet. Sci., 6(1), 457–494, doi:10.1146/annurev.ea.06.050178.002325, 1978.

Dolman, A. M. and Laepple, T.: Sedproxy: a forward model for sediment archived climate proxies, Climate of the Past Discussions, 1–31, doi:10.5194/cp-2018-13, 2018.

Emiliani, C. and Milliman, J. D.: Deep-sea sediments and their geological record, Earth-Science Reviews, 1(2–3), 105–132, doi:10.1016/0012-8252(66)90002-X, 1966.

Ericson, D. B., Broecker, W. S., Kulp, J. L. and Wollin, G.: Late-Pleistocene Climates and Deep-Sea Sediments, Science, 124(3218), 385–389, doi:10.1126/science.124.3218.385, 1956.

Erlenkeuser, H.: 14C age and vertical mixing of deep-sea sediments, Earth and Planetary Science Letters, 47(3), 319–326, doi:10.1016/0012-821X(80)90018-7, 1980.

Guillou, H., Singer, B. S., Laj, C., Kissel, C., Scaillet, S. and Jicha, B. R.: On the age of the Laschamp geomagnetic excursion, Earth and Planetary Science Letters, 227(3), 331–343, doi:10.1016/j.epsl.2004.09.018, 2004.

Guinasso, N. L. and Schink, D. R.: Quantitative estimates of biological mixing rates in abyssal sediments, J. Geophys. Res., 80(21), 3032–3043, doi:10.1029/JC080i021p03032, 1975.

Keigwin, L. D. and Guilderson, T. P.: Bioturbation artifacts in zero-age sediments, Paleoceanography, 24(4), doi:10.1029/2008PA001727, 2009.

Laj, C., Guillou, H. and Kissel, C.: Dynamics of the earth magnetic field in the 10–75 kyr period comprising the Laschamp and Mono Lake excursions: New results from the French Chaîne des Puys in a global perspective, Earth and Planetary Science Letters, 387, 184–197, doi:10.1016/j.epsl.2013.11.031, 2014.

Le, J. and Shackleton, N. J.: Carbonate Dissolution Fluctuations in the Western Equatorial Pacific During the Late Quaternary, Paleoceanography, 7(1), 21–42, doi:10.1029/91PA02854, 1992.

Lougheed, B. C.: SEAMUS (v1.0): a Δ14C-enabled, single-specimen sediment accumulation simulator, Geoscientific Model Development, doi:10.5194/gmd-2019-155, 2019.

Lougheed, B. C. and Obrochta, S. P.: MatCal: Open Source Bayesian 14C Age Calibration in Matlab, Journal of Open Research Software, 4, doi:10.5334/jors.130, 2016.

Lougheed, B. C., Snowball, I., Moros, M., Kabel, K., Muscheler, R., Virtasalo, J. J. and Wacker, L.: Using an independent geochronology based on palaeomagnetic secular variation (PSV) and atmospheric Pb deposition to date Baltic Sea sediments and infer 14C reservoir age, Quaternary Science Reviews, 42, 43–58, 2012.

Lougheed, B. C., Metcalfe, B., Ninnemann, U. S. and Wacker, L.: Moving beyond the age-depth model paradigm in deep sea palaeoclimate archives: dual radiocarbon and stable isotope analysis on single foraminifera, Climate of the Past, 14, 515–526, doi:10.5194/cp-2017-119, 2018.

Löwemark, L. and Grootes, P. M.: Large age differences between planktic foraminifers caused by abundance variations and Zoophycos bioturbation., Paleoceanography, 19(2), PA2001, doi:10.1029/2003PA000949, 2004.

Löwemark, L., Konstantinou, K. I. and Steinke, S.: Bias in foraminiferal multispecies reconstructions of paleohydrographic conditions caused by foraminiferal abundance variations and bioturbational mixing: A model approach, Marine Geology, 256(1–4), 101–106, doi:10.1016/j.margeo.2008.10.005, 2008.

Mekhaldi, F., Muscheler, R., Adolphi, F., Aldahan, A., Beer, J., McConnell, J. R., Possnert, G., Sigl, M., Svensson, A., Synal, H.-A., Welten, K. C. and Woodruff, T. E.: Multiradionuclide evidence for the solar origin of the cosmic-ray events of AD 774/5 and 993/4, Nature Communications, 6, 8611, doi:10.1038/ncomms9611, 2015.

Miyake, F., Nagaya, K., Masuda, K. and Nakamura, T.: A signature of cosmic-ray increase in AD 774–775 from tree rings in Japan, Nature, 486(7402), 240–242, doi:10.1038/nature11123, 2012.

Miyake, F., Jull, A. J. T., Panyushkina, I. P., Wacker, L., Salzer, M., Baisan, C. H., Lange, T., Cruz, R., Masuda, K. and Nakamura, T.: Large 14C excursion in 5480 BC indicates an abnormal sun in the mid-Holocene, PNAS, 114(5), 881–884, doi:10.1073/pnas.1613144114, 2017.

Müller, P. J. and Suess, E.: Productivity, sedimentation rate, and sedimentary organic matter in the oceans—I. Organic carbon preservation, Deep Sea Research Part A. Oceanographic Research Papers, 26(12), 1347–1362, doi:10.1016/0198-0149(79)90003-7, 1979.

Muscheler, R., Adolphi, F. and Svensson, A.: Challenges in 14C dating towards the limit of the method inferred from anchoring a floating tree ring radiocarbon chronology to ice core records around the Laschamp geomagnetic field minimum, Earth and Planetary Science Letters, 394, 209–215, doi:10.1016/j.epsl.2014.03.024, 2014.

Nayudu, Y. R.: Volcanic ash deposits in the Gulf of Alaska and problems of correlation of deep-sea ash deposits, Marine Geology, 1(3), 194–212, doi:10.1016/0025-3227(64)90058-1, 1964.

Olausson, E.: Studies of deep-sea cores. Sediment cores from the Mediterranean Sea and the Red Sea, Report of the Swedish Deep Sea Expedition 1947-48, 8, 337–391, 1961.

Parker, F. L. and Berger, W. H.: Faunal and solution patterns of planktonic Foraminifera in surface sediments of the South Pacific, Deep Sea Research and Oceanographic Abstracts, 18(1), 73–107, doi:10.1016/0011-7471(71)90017-9, 1971.

Paull, C. K., Hills, S. J., Thierstein, H. R. and Bonani, G.: 14C Offsets and Apparently Non-synchronous d180 Stratigraphies between Nannofossil and Foraminiferal Pelagic Carbonates, Quaternary Research, 35(2), 274–290, 1991.

Peng, T.-H. and Broecker, W. S.: The impacts of bioturbation on the age difference between benthic and planktonic foraminifera in deep sea sediments, Nuclear Instruments and Methods in Physics Research Section B: Beam Interactions with Materials and Atoms, 5(2), 346–352, 1984.

Peng, T.-H., Broecker, W. S. and Berger, W. H.: Rates of benthic mixing in deep-sea sediment as determined by radioactive tracers, Quaternary Research, 11(1), 141–149, 1979.

Pisias, N. G.: Geologic time series from deep-sea sediments: Time scales and distortion by bioturbation, Marine Geology, 51(1–2), 99–113, 1983.

Reimer, P. J., Bard, E., Bayliss, A., Beck, J. W., Blackwell, P. G., Ramsey, C. B., Buck, C. E., Cheng, H., Edwards, R. L., Friedrich, M., Grootes, P. M., Guilderson, T. P., Haflidason, H., Hajdas, I., Hatté, C., Heaton, T. J., Hoffmann, D. L., Hogg, A. G., Hughen, K. A., Kaiser, K. F., Kromer, B., Manning, S. W., Niu, M., Reimer, R. W., Richards, D. A., Scott, E. M., Southon, J. R., Staff, R. A., Turney, C. S. M. and van der Plicht, J.: IntCal13 and Marine13 Radiocarbon Age Calibration Curves 0–50,000 Years cal BP, Radiocarbon, 55(04), 1869–1887, 2013.

Rubin, M. and Suess, H. E.: U.S. Geological Survey Radiocarbon Dates 11., Science, 121, 481–488, 1955.

Ruddiman, W., Jones, G., Peng, T.-H., Glover, L., Glass, B. and Liebertz, P.: Tests for size and shape dependency in deep-sea mixing, Sedimentary Geology, 25(4), 257–276, 1980.

Ruddiman, W. F. and Glover, L. K.: Vertical mixing of ice-rafted volcanic ash in North Atlantic sediments, Geological Society of America Bulletin, 83(9), 2817–2836, 1972.

Ruddiman, W. F. and Heezen, B. C.: Differential solution of Planktonic Foraminifera, Deep Sea Research and Oceanographic Abstracts, 14(6), 801–808, doi:10.1016/S0011-7471(67)80016-0, 1967.

Ruff, M., Szidat, S., Gäggeler, H. W., Suter, M., Synal, H.-A. and Wacker, L.: Gaseous radiocarbon measurements of small samples, Nuclear Instruments and Methods in Physics Research Section B:

Beam Interactions with Materials and Atoms, 268(7), 790–794, doi:10.1016/j.nimb.2009.10.032, 2010.

Schiffelbein, P.: Effect of benthic mixing on the information content of deep-sea stratigraphical signals, Nature, 311(5987), 651, doi:10.1038/311651a0, 1984.

Siegenthaler, U., Heimann, M. and Oeschger, H.: 14C Variations Caused by Changes in the Global Carbon Cycle, Radiocarbon, 22(2), 177–191, doi:10.1017/S0033822200009449, 1980.

Stuiver, M. and Polach, H. A.: Discussion: Reporting of 14C data, Radiocarbon, 19(03), 355–363, 1977.

Suess, H. E.: Radiocarbon Concentration in Modern Wood, Science, 122(3166), 415–417, doi:10.1126/science.122.3166.415-a, 1955.

Suess, H. E.: Secular variations of the cosmic-ray-produced carbon 14 in the atmosphere and their interpretations, Journal of Geophysical Research (1896-1977), 70(23), 5937–5952, doi:10.1029/JZ070i023p05937, 1965.

Teal, L. R., Bulling, M. T., Parker, E. R. and Solan, M.: Global patterns of bioturbation intensity and mixed depth of marine soft sediments, Aquatic Biology, 2(3), 207–218, doi:10.3354/ab00052, 2008.

Trauth, M. H.: TURBO2: A MATLAB simulation to study the effects of bioturbation on paleoceanographic time series, Computers & Geosciences, 61, 1–10, doi:10.1016/j.cageo.2013.05.003, 2013.

Trauth, M. H., Sarnthein, M. and Arnold, M.: Bioturbational mixing depth and carbon flux at the seafloor, Paleoceanography, 12(3), 517–526, 1997.

de Vries, H.: Variation in concentration of radiocarbon with time and location on Earth, Proceedings of the Koninklijke Nederlandse Akademie van Wetenschappen B, 61, 94–108, 1958.

Wacker, L., Fülöp, R.-H., Hajdas, I., Molnár, M. and Rethemeyer, J.: A novel approach to process carbonate samples for radiocarbon measurements with helium carrier gas, Nuclear Instruments and Methods in Physics Research Section B: Beam Interactions with Materials and Atoms, 294, 214–217, doi:10.1016/j.nimb.2012.08.030, 2013a.

Wacker, L., Lippold, J., Molnár, M. and Schulz, H.: Towards radiocarbon dating of single foraminifera with a gas ion source, Nuclear Instruments and Methods in Physics Research Section B: Beam Interactions with Materials and Atoms, 294, 307–310, doi:10.1016/j.nimb.2012.08.038, 2013b.

First downcore occurrence of ^{14}C-dead foraminifera								
	0 % broken foraminifera scenario				*10% broken foraminifera scenario*			
	Discrete depth (cm)	*Median true age (yr)*	*AMS ^{14}C age (^{14}C yr BP)*	*Median ^{14}C calibrated age (cal yr BP)*	*Discrete depth (cm)*	*Median true age (yr)*	*AMS ^{14}C age (^{14}C yr BP)*	*Median ^{14}C calibrated age (cal yr BP)*
SAR 5 cm ka^{-1} BD 10 cm	133-134	26110	22647	26493	237-238	46690	44096	46833
SAR 10 cm ka^{-1} BD 10 cm	375-376	37250	33747	37654	486-487	48260	45422	48396
SAR 20 cm ka^{-1} BD 10 cm	900-901	44855	41973	45002	986-987	49125	46090	49186
SAR 40 cm ka^{-1} BD 10 cm	1894-1895	47285	44582	47383	1987-1988	49585	46455	49544
SAR 60 cm ka^{-1} BD 10 cm	2866-2867	47725	44912	47775	2986-2987	49710	46556	49621

Table 1. The first downcore discrete-depth where ^{14}C-dead whole foraminifera occur (i.e $n_{dead} \geq 1$) for the various SAR and broken foraminifera scenarios simulated in this study. Also shown are the simulated median true ages, AMS ^{14}C ages and median ^{14}C calibrated ages corresponding to the discrete depth. The simulation blank value is set at 46806 ^{14}C yr BP (see Section 2.1), thus any single foraminifera with a ^{14}C age older than that blank value are assumed ^{14}C-dead.

Multiple constant SAR scenarios with:
constant BD of 10 cm, constant abundance of 100% and 0% broken foraminifera

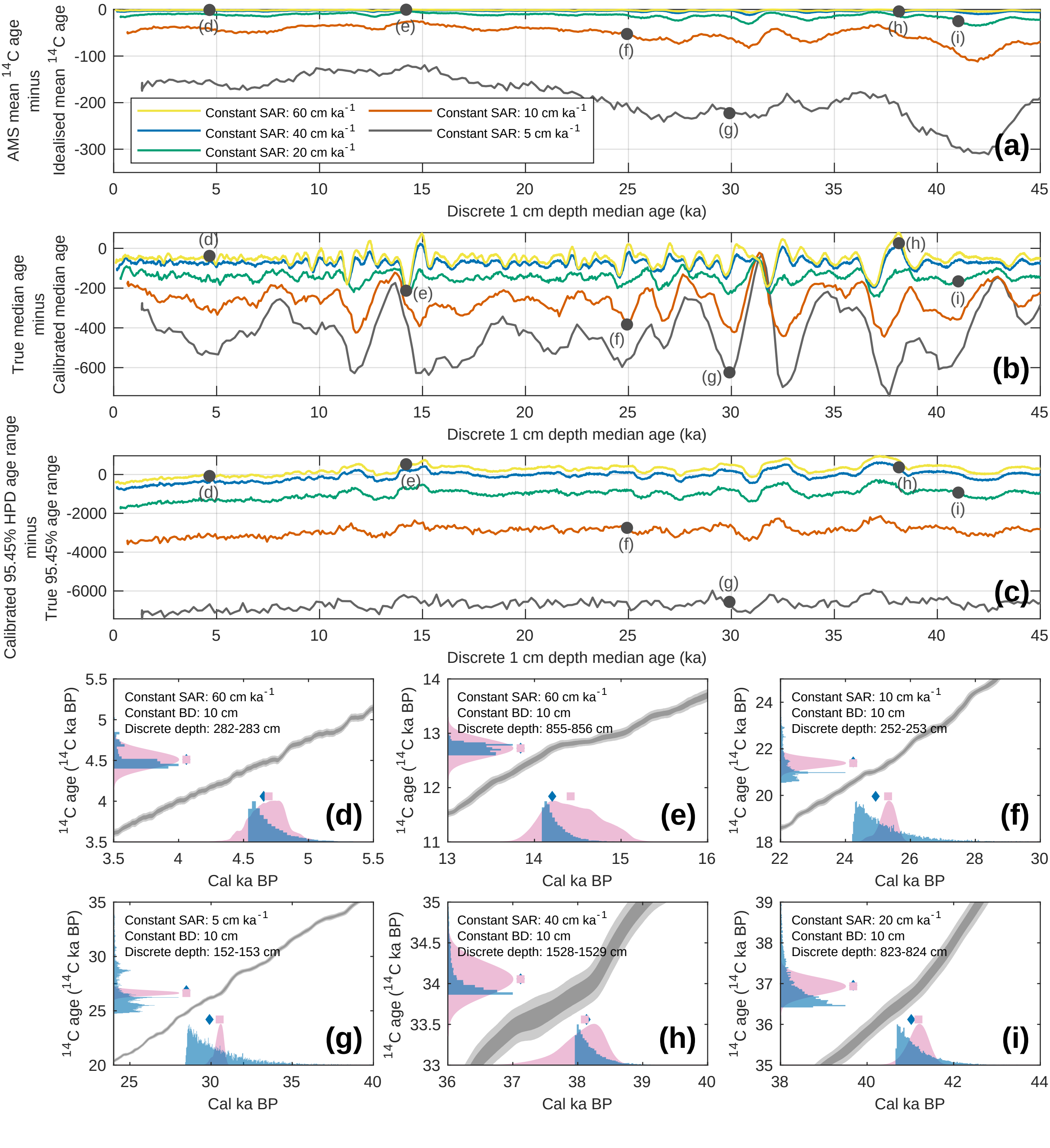

Figure 1. (a-c) Overview of downcore, 1 cm discrete-depth sediment archive simulation results involving multiple constant SAR scenarios (5, 10, 20, 40 and 60 cm ka^{-1}) with constant BD of 10 cm, constant species abundance of 100% and 0% broken foraminifera. All discrete-depth results are plotted against their true median age on the x-axes. **(a)** The offset between mean AMS (i.e. laboratory) conventional ^{14}C age and the true mean ^{14}C age. **(b)** The offset between the true median age and the calibrated median age (i.e. that derived from the ^{14}C dating and calibration process). **(c)** The difference between the calibrated highest posterior density (HPD) 95.45% age range (i.e that derived from the 14C dating and calibration process) and the true 95.45% age range of the sediment. **(d, e, f, g, h, i)** A visualisation of ^{14}C calibration skill for select discrete-depth subsamples from various scenarios indicated on the figure panels. The blue histograms represent the single-specimen simulation output: on the x-axis the true age distribution of the single specimens (with the blue diamond corresponding to the median true age), and on the y-axis the corresponding ^{14}C age distribution of the single specimens (with the blue diamond corresponding to the mean ^{14}C age). All histograms are shown using 30 (^{14}C) year bins. The pink normal distribution on the y-axis represents the idealised AMS ^{14}C determination of the single specimens, where the pink square corresponds to the expected mean conventional ^{14}C age. The pink probability distribution on the x-axis represents the calibrated age PDF arising from the calibration of the aforementioned AMS ^{14}C determination using *Marine13* (Reimer et al, 2013) and *MatCal* (Lougheed and Obrochta, 2016). Also shown, for reference, are the *Marine13* calibration curve 1σ (dark grey) and 2σ (light grey) confidence intervals.

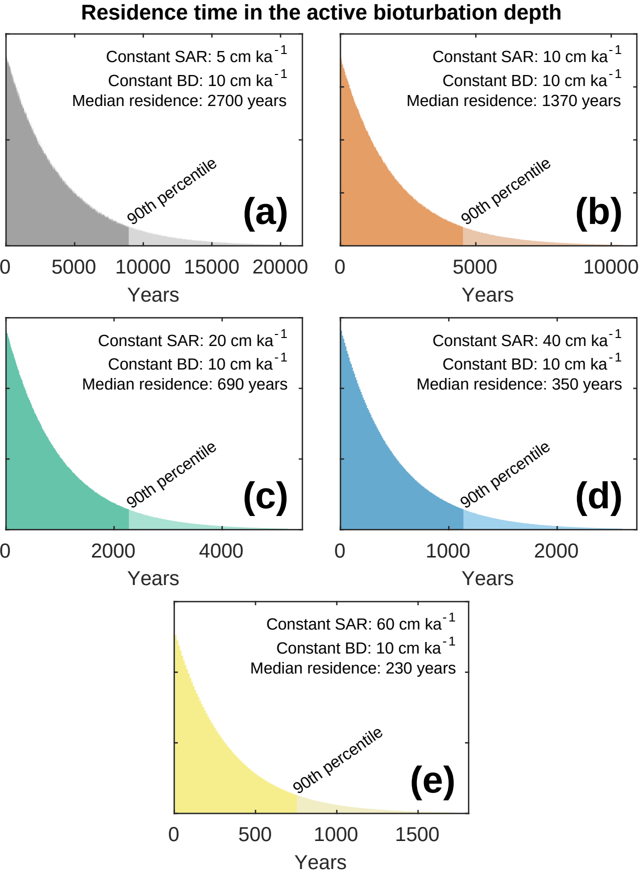
Residence time in the active bioturbation depth
Constant SAR: 5 cm ka-1
Constant BD: 10 cm ka-1
Median residence: 2700 years
90th percentile
(a)
0
5000
10000
15000
20000
Years
Constant SAR: 10 cm ka-1
Constant BD: 10 cm ka-1
Median residence: 1370 years
90th percentile
(b)
0
5000
10000
Years
Constant SAR: 20 cm ka-1
Constant BD: 10 cm ka-1
Median residence: 690 years
90th percentile
(c)
0
2000
4000
Years
Constant SAR: 40 cm ka-1
Constant BD: 10 cm ka-1
Median residence: 350 years
90th percentile
(d)
0
1000
2000
Years
Constant SAR: 60 cm ka-1
Constant BD: 10 cm ka-1
Median residence: 230 years
90th percentile
(e)
0
500
1000
1500
Years

Figure 2. An overview of residence time of single foraminifera within the active BD for the various simulation scenarios detailed in Fig. 1, i.e. with a constant BD of 10 cm and a SAR of **(a)** 5 cm ka^{-1} **(b)** 10 cm ka^{-1} **(c)** 20 cm ka^{-1} **(d)** 40 cm ka^{-1} **(e)** 60 cm ka^{-1}.

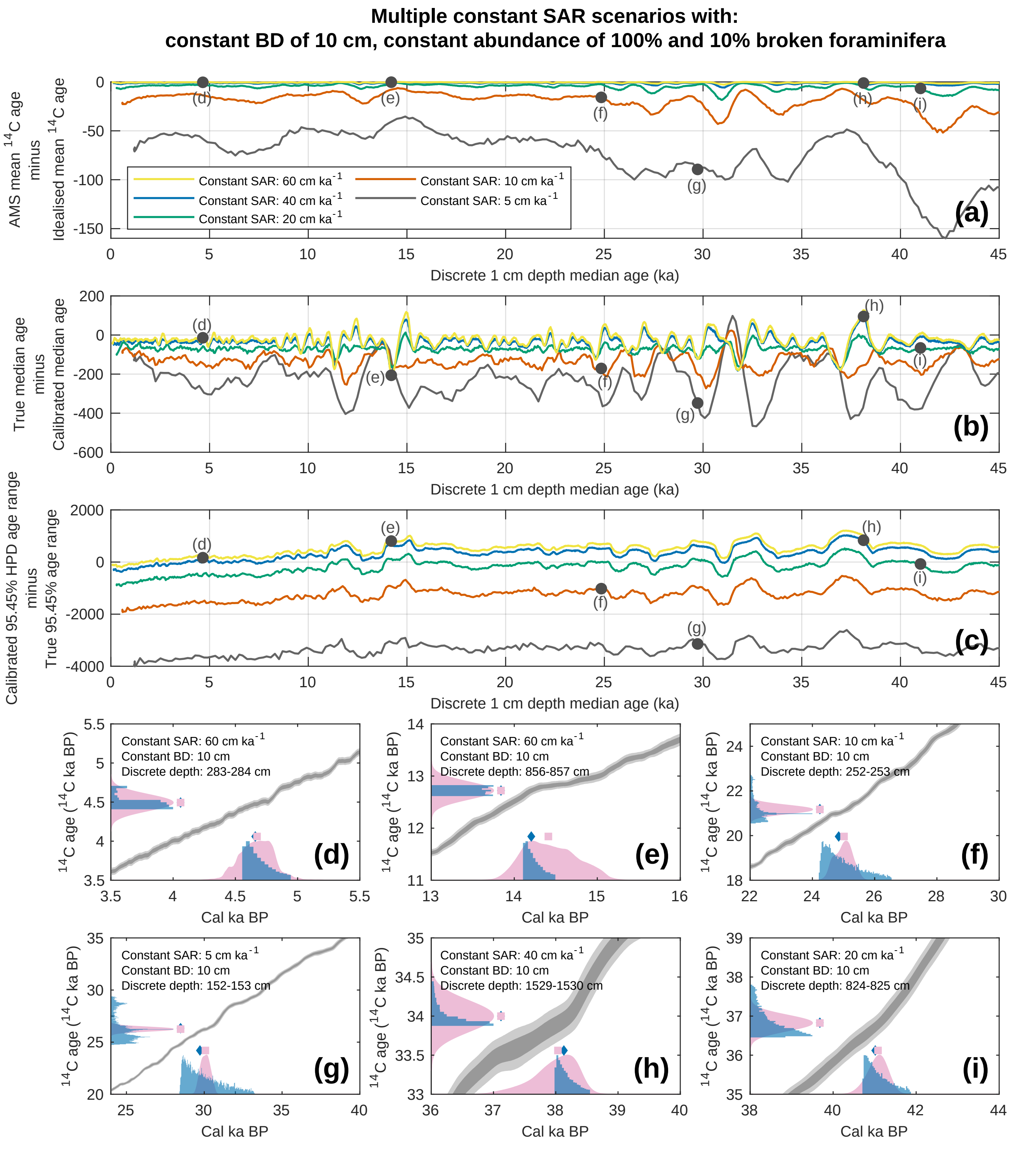

Multiple constant SAR scenarios with:
constant BD of 10 cm, constant abundance of 100% and 10% broken foraminifera
AMS mean 14C age minus Idealised mean 14C age
Constant SAR: 60 cm ka-1
Constant SAR: 40 cm ka-1
Constant SAR: 20 cm ka-1
Constant SAR: 10 cm ka-1
Constant SAR: 5 cm ka-1
(a)
Discrete 1 cm depth median age (ka)
True median age minus Calibrated median age
(b)
Calibrated 95.45% HPD age range minus True 95.45% age range
(c)
(d)
(e)
(f)
(g)
(h)
(i)
14C age (14C ka BP)
Cal ka BP
Constant SAR: 60 cm ka-1
Constant BD: 10 cm
Discrete depth: 283-284 cm
Constant SAR: 60 cm ka-1
Constant BD: 10 cm
Discrete depth: 856-857 cm
Constant SAR: 10 cm ka-1
Constant BD: 10 cm
Discrete depth: 252-253 cm
Constant SAR: 5 cm ka-1
Constant BD: 10 cm
Discrete depth: 152-153 cm
Constant SAR: 40 cm ka-1
Constant BD: 10 cm
Discrete depth: 1529-1530 cm
Constant SAR: 20 cm ka-1
Constant BD: 10 cm
Discrete depth: 824-825 cm

Figure 3. (a-c) Overview of downcore, 1 cm discrete-depth sediment archive simulation results involving multiple constant SAR scenarios (5, 10, 20, 40 and 60 cm ka^{-1}) with constant BD of 10 cm, constant species abundance of 100% and 10% broken foraminifera. All discrete-depth results are plotted against their true median age on the x-axes. **(a)** The offset between mean AMS (i.e. laboratory) conventional ^{14}C age and the idealised mean ^{14}C age. **(b)** The offset between the true median age and the calibrated median age (i.e. that derived from the ^{14}C dating and calibration process). **(c)** The difference between the calibrated highest posterior density (HPD) 95.45% age range (i.e that derived from the 14C dating and calibration process) and the true 95.45% age range of the sediment. **(d, e, f, g, h, i)** A visualisation of ^{14}C calibration skill for select discrete-depth subsamples from various scenarios indicated on the figure panels. The blue histograms represent the single-specimen simulation output: on the x-axis the true age distribution of the single specimens (with the blue diamond corresponding to the median true age), and on the y-axis the corresponding ^{14}C age distribution of the single specimens (with the blue diamond corresponding to the mean ^{14}C age). All histograms are shown using 30 (^{14}C) year bins. The pink normal distribution on the y-axis represents the idealised AMS ^{14}C determination of the single specimens, where the pink square corresponds to the expected mean conventional ^{14}C age. The pink probability distribution on the x-axis represents the calibrated age PDF arising from the calibration of the aforementioned AMS ^{14}C determination using *Marine13* (Reimer et al, 2013) and *MatCal* (Lougheed and Obrochta, 2016). Also shown, for reference, are the *Marine13* calibration curve 1σ (dark grey) and 2σ (light grey) confidence intervals.

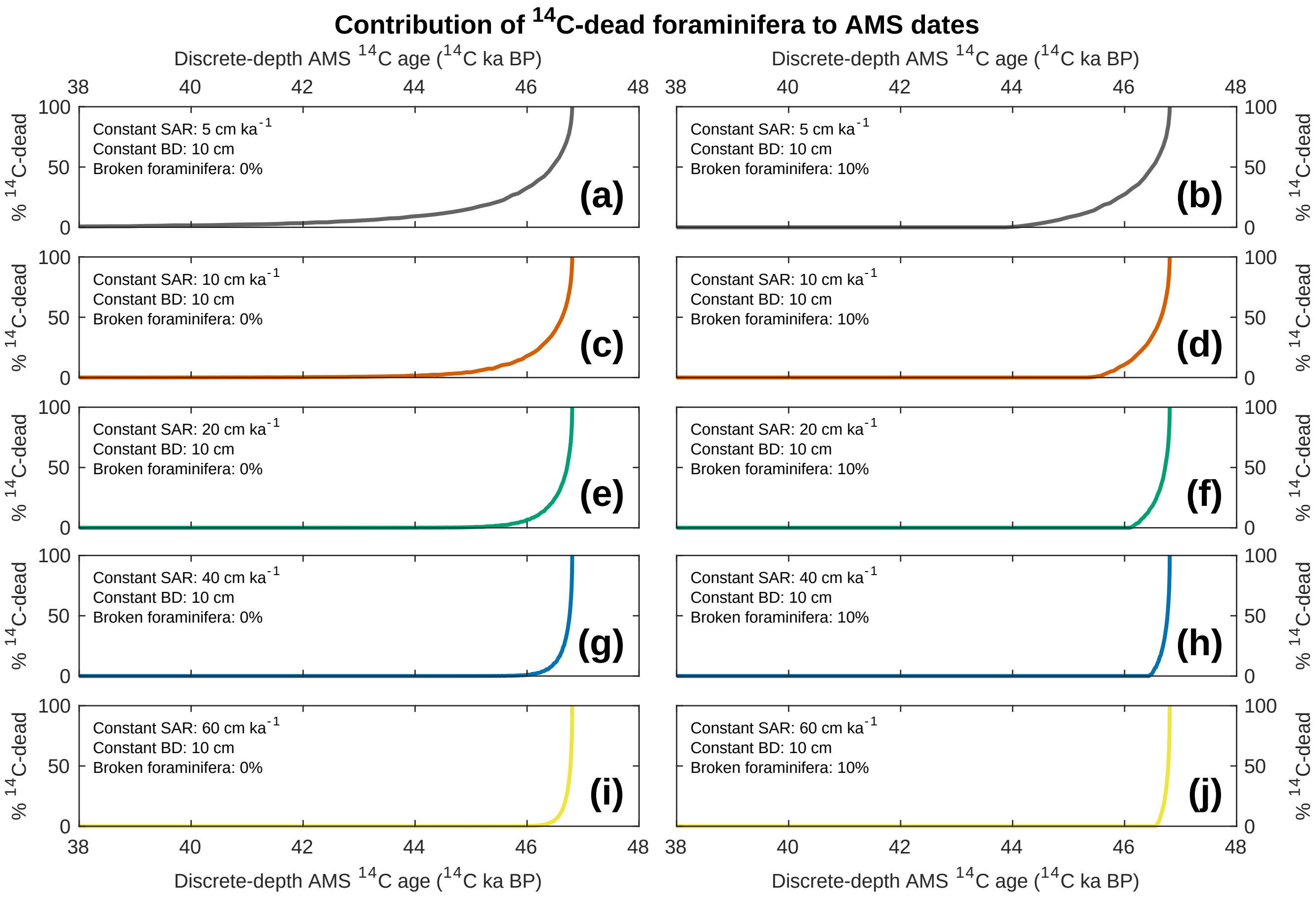
Contribution of 14C-dead foraminifera to AMS dates
Discrete-depth AMS 14C age (14C ka BP)
% 14C-dead
Constant SAR: 5 cm ka-1
Constant BD: 10 cm
Broken foraminifera: 0%
(a)
Constant SAR: 5 cm ka-1
Constant BD: 10 cm
Broken foraminifera: 10%
(b)
Constant SAR: 10 cm ka-1
Constant BD: 10 cm
Broken foraminifera: 0%
(c)
Constant SAR: 10 cm ka-1
Constant BD: 10 cm
Broken foraminifera: 10%
(d)
Constant SAR: 20 cm ka-1
Constant BD: 10 cm
Broken foraminifera: 0%
(e)
Constant SAR: 20 cm ka-1
Constant BD: 10 cm
Broken foraminifera: 10%
(f)
Constant SAR: 40 cm ka-1
Constant BD: 10 cm
Broken foraminifera: 0%
(g)
Constant SAR: 40 cm ka-1
Constant BD: 10 cm
Broken foraminifera: 10%
(h)
Constant SAR: 60 cm ka-1
Constant BD: 10 cm
Broken foraminifera: 0%
(i)
Constant SAR: 60 cm ka-1
Constant BD: 10 cm
Broken foraminifera: 10%
(j)

Figure 4. An estimation of the contribution of ^{14}C-blank foraminifera to discrete-depth subsamples plotted against their apparent AMS ^{14}C mean age. Based on the simulation scenarios detailed in Fig. 1 and Fig 3 with a constant BD of 10 cm and **(a)** SAR of 5 cm ka^{-1} and 0% broken foraminifera, **(b)** SAR of 5 cm ka^{-1} and 10% broken foraminifera, **(c)** SAR of 10 cm ka^{-1} and 0% broken foraminifera **(d)** SAR of 10 cm ka^{-1} and 10% broken foraminifera, **(e)** SAR of 20 cm ka^{-1} and 0% broken foraminifera, **(f)** SAR of 20 cm ka^{-1} and 10% broken foraminifera, **(g)** SAR of 40 cm ka^{-1} and 0% broken foraminifera, **(h)** SAR of 40 cm ka^{-1} and 10% broken foraminifera, **(i)** SAR of 60 cm ka^{-1} and 0% broken foraminifera, **(j)** SAR of 60 cm ka^{-1} and 10% broken foraminifera.

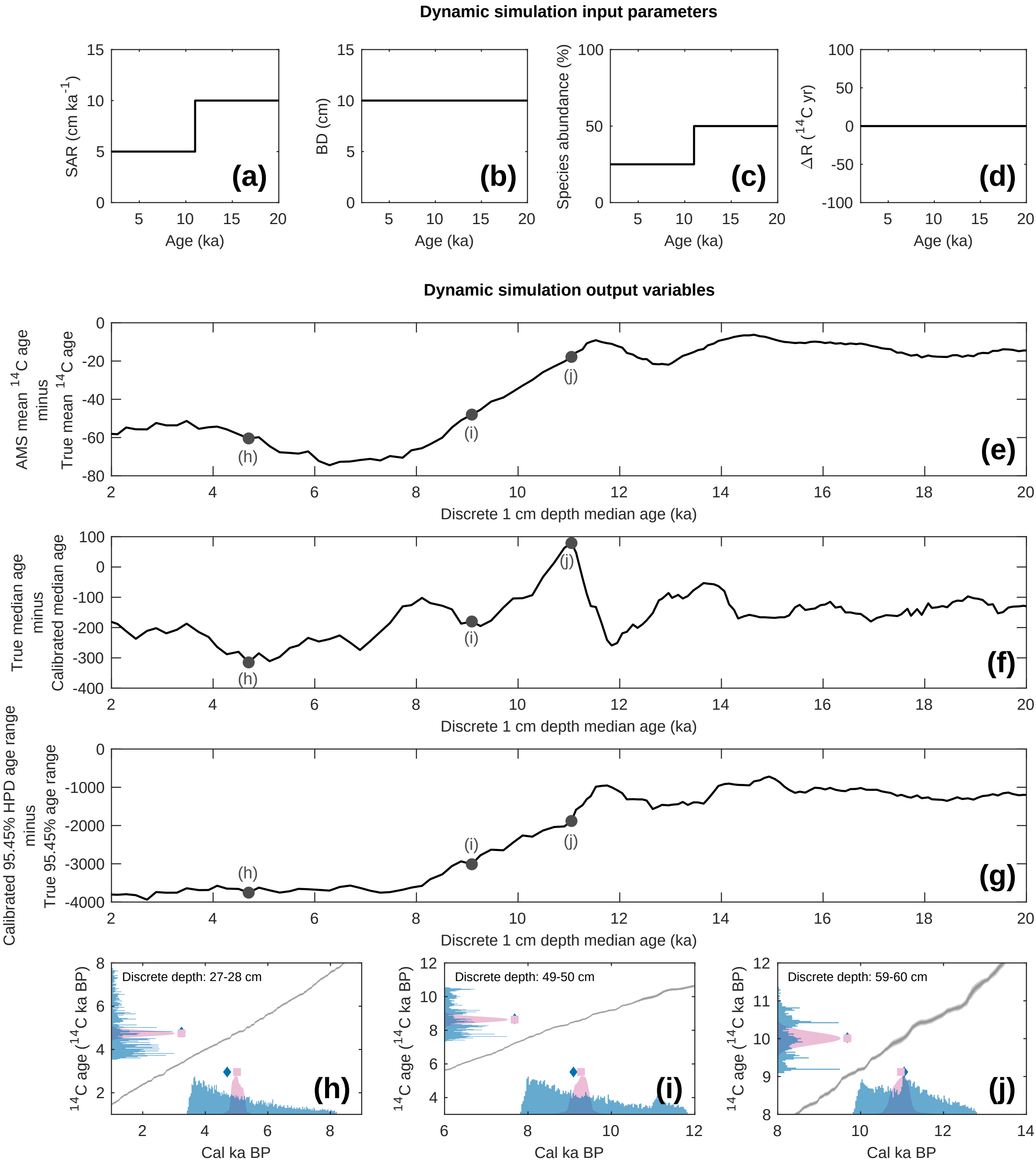
Dynamic simulation input parameters
SAR (cm ka-1)
(a)
BD (cm)
(b)
Species abundance (%)
(c)
ΔR (14C yr)
(d)
Age (ka)
Dynamic simulation output variables
AMS mean 14C age minus True mean 14C age
(e)
Discrete 1 cm depth median age (ka)
True median age minus Calibrated median age
(f)
Calibrated 95.45% HPD age range minus True 95.45% age range
(g)
(h)
(i)
(j)
Discrete depth: 27-28 cm
Discrete depth: 49-50 cm
Discrete depth: 59-60 cm
14C age (14C ka BP)
Cal ka BP

Figure 5. A simulation scenario with custom input for **(a)** SAR, **(b)** BD, **(c)** species abundance, **(d)** reservoir age. A constant broken foraminifera percentage of 10% is applied. **(e)** The resulting offset between mean AMS (i.e. laboratory) conventional ^{14}C age and the idealised mean ^{14}C age. **(f)** The offset between the true median age and the calibrated median age (i.e. that derived from the ^{14}C dating and calibration process). **(g)** The difference between the calibrated highest posterior density (HPD) 95.45% age range (i.e that derived from the 14C dating and calibration process) and the true 95.45% age range of the sediment. **(h, i, j)** A visualisation of ^{14}C calibration skill for select discrete-depth subsamples from the simulation scenario with custom input. The blue histograms represent the single-specimen simulation output: on the x-axis the true age distribution of the single specimens (with the blue diamond corresponding to the median true age), and on the y-axis the corresponding ^{14}C age distribution of the single specimens (with the blue diamond corresponding to the mean ^{14}C age). All histograms are shown using 30 (^{14}C) year bins. The pink normal distribution on the y-axis represents the idealised AMS ^{14}C determination of the single specimens, where the pink square corresponds to the expected mean conventional ^{14}C age. The pink probability distribution on the x-axis represents the calibrated age PDF arising from the calibration of the aforementioned AMS ^{14}C determination using *Marine13* (Reimer et al, 2013) and *MatCal* (Lougheed and Obrochta, 2016). Also shown, for reference, are the *Marine13* calibration curve 1σ (dark grey) and 2σ (light grey) confidence intervals.

Constant SAR of 5 cm ka^{-1} with:
constant BD of 10 cm, constant abundance of 100% and 0% broken foraminifera

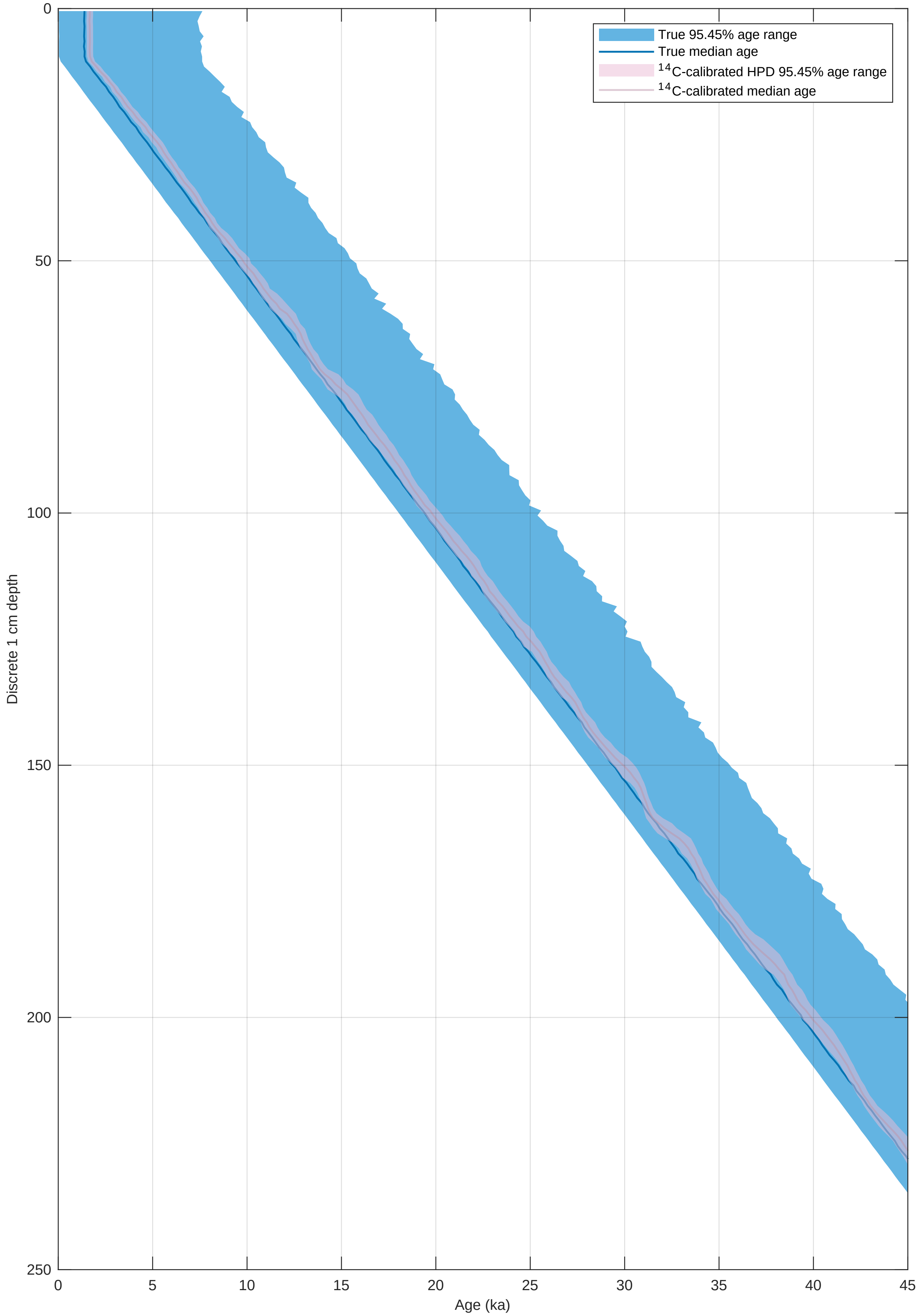

Figure S1. Simulated 1 cm discrete-depth 95.45% true age range (light blue), true median age (dark blue), ^{14}C-calibrated 95.45% HPD age range (light pink) and ^{14}C-calibrated median age (dark pink for whole foraminifera in a simulation scenario with a constant SAR of 5 cm ka-1, constant BD of 10 cm and 0% broken foraminifera.

Constant SAR of 10 cm ka^{-1} with:
constant BD of 10 cm, constant abundance of 100% and 0% broken foraminifera

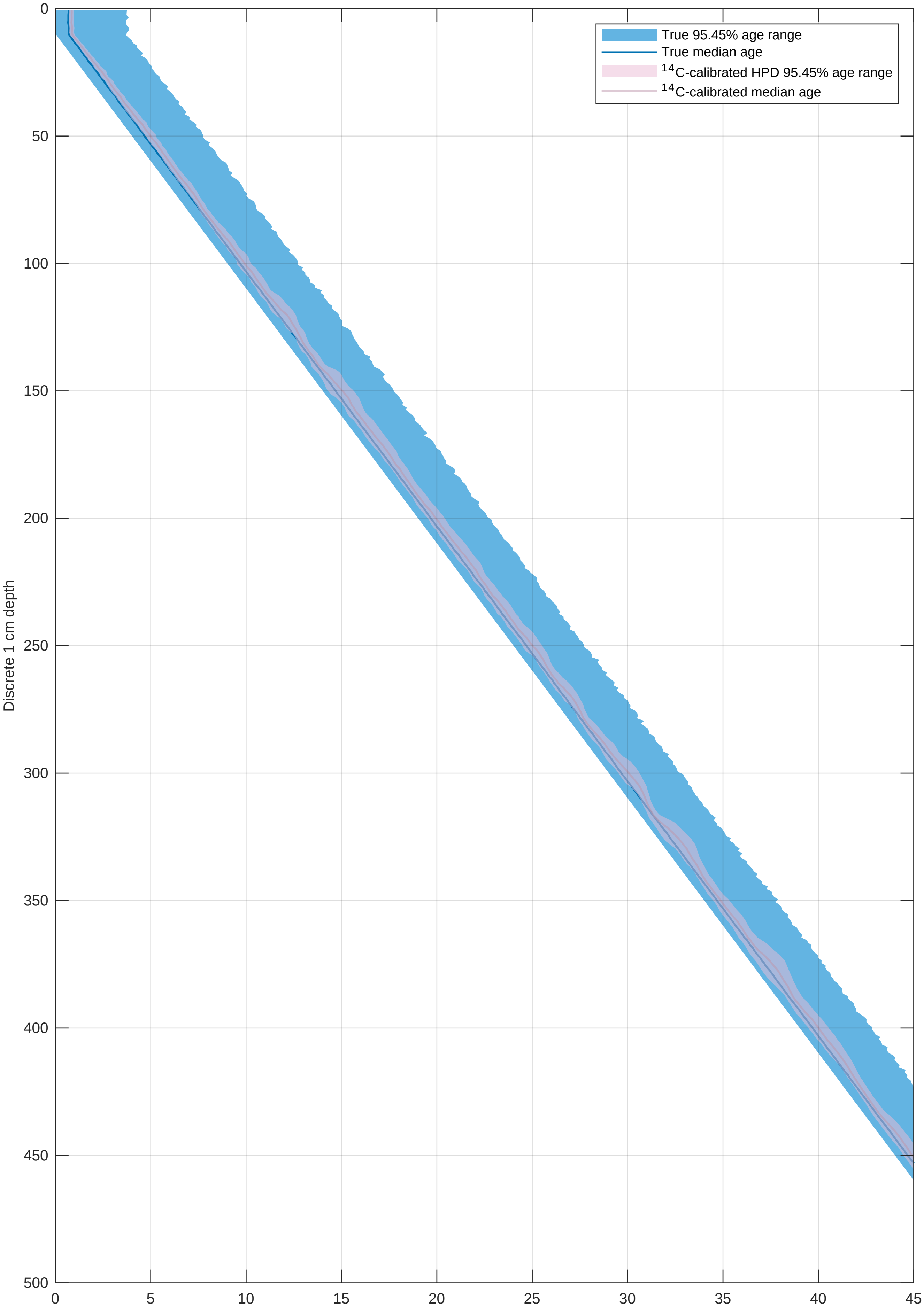

Figure S2. Simulated 1 cm discrete-depth 95.45% true age range (light blue), true median age (dark blue), ^{14}C-calibrated 95.45% HPD age range (light pink) and ^{14}C-calibrated median age (dark pink for whole foraminifera in a simulation scenario with a constant SAR of 10 cm ka-1, constant BD of 10 cm and 0% broken foraminifera.

Constant SAR of 20 cm ka^{-1} with:
constant BD of 10 cm, constant abundance of 100% and 0% broken foraminifera

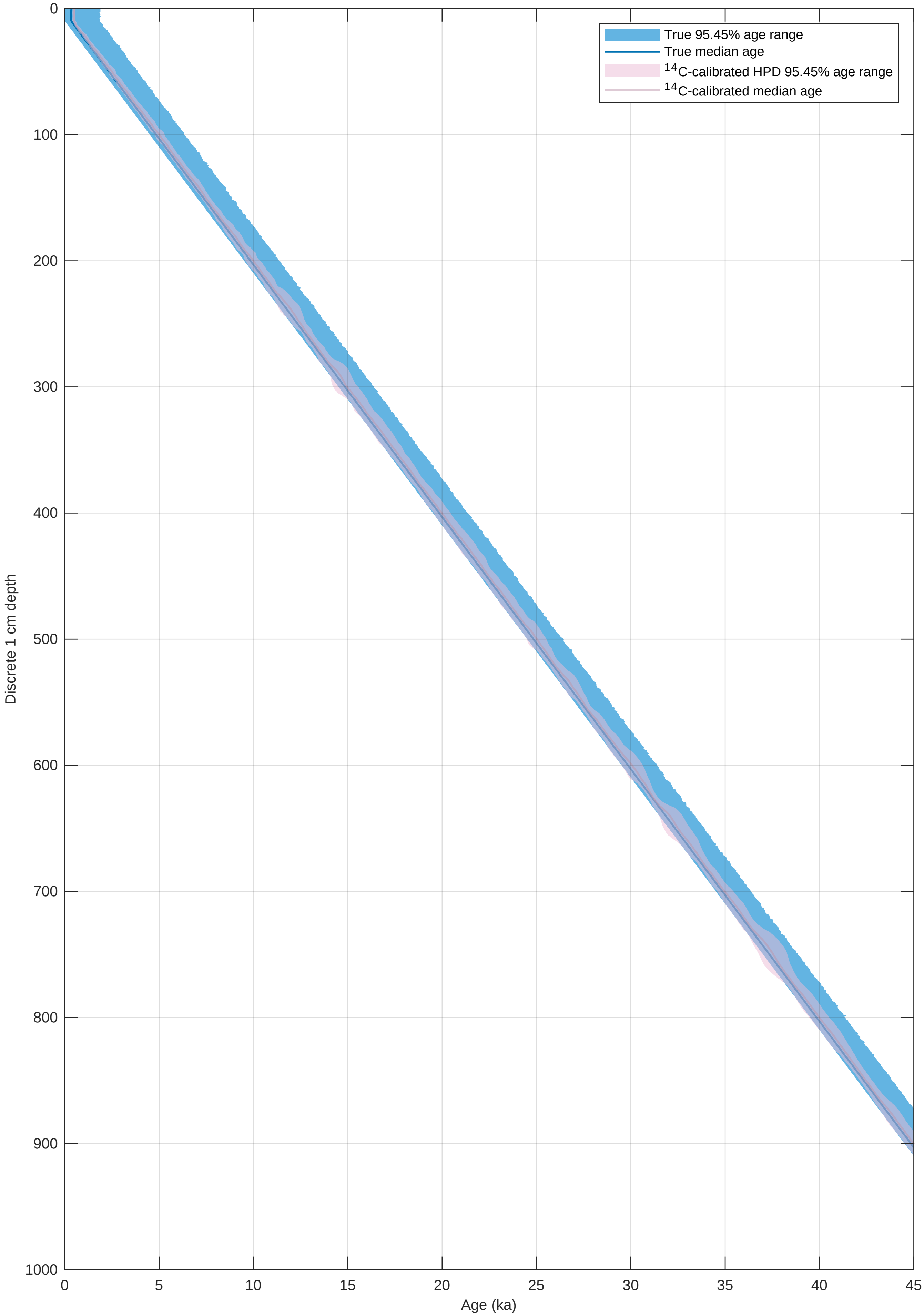

Figure S3. Simulated 1 cm discrete-depth 95.45% true age range (light blue), true median age (dark blue), ^{14}C-calibrated 95.45% HPD age range (light pink) and ^{14}C-calibrated median age (dark pink for whole foraminifera in a simulation scenario with a constant SAR of 20 cm ka-1, constant BD of 10 cm and 0% broken foraminifera.

Constant SAR of 40 cm ka^{-1} with:
constant BD of 10 cm, constant abundance of 100% and 0% broken foraminifera

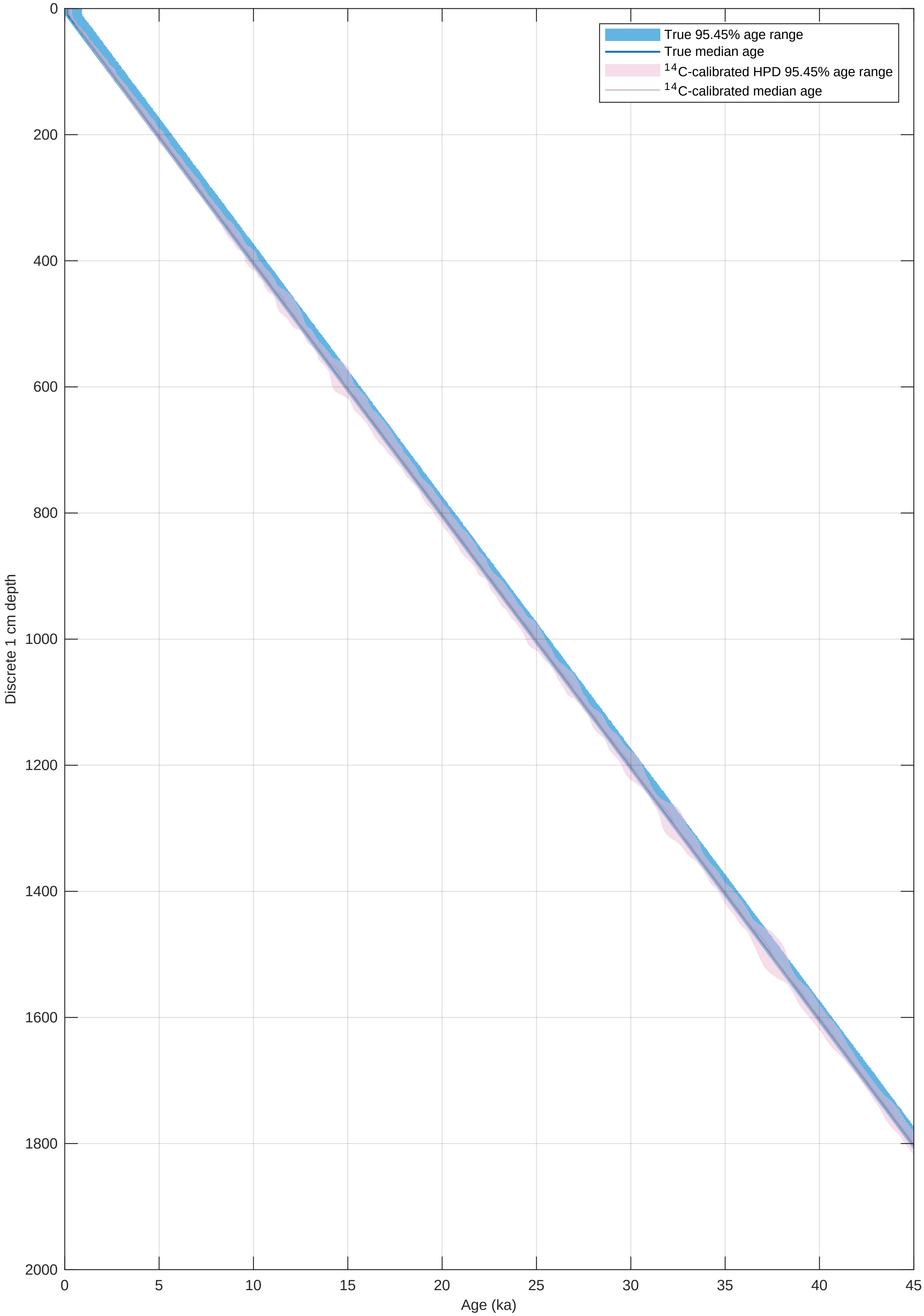

Figure S4. Simulated 1 cm discrete-depth 95.45% true age range (light blue), true median age (dark blue), ^{14}C-calibrated 95.45% HPD age range (light pink) and ^{14}C-calibrated median age (dark pink for whole foraminifera in a simulation scenario with a constant SAR of 40 cm ka-1, constant BD of 10 cm and 0% broken foraminifera.

Constant SAR of 60 cm ka^{-1} with:
constant BD of 10 cm, constant abundance of 100% and 0% broken foraminifera

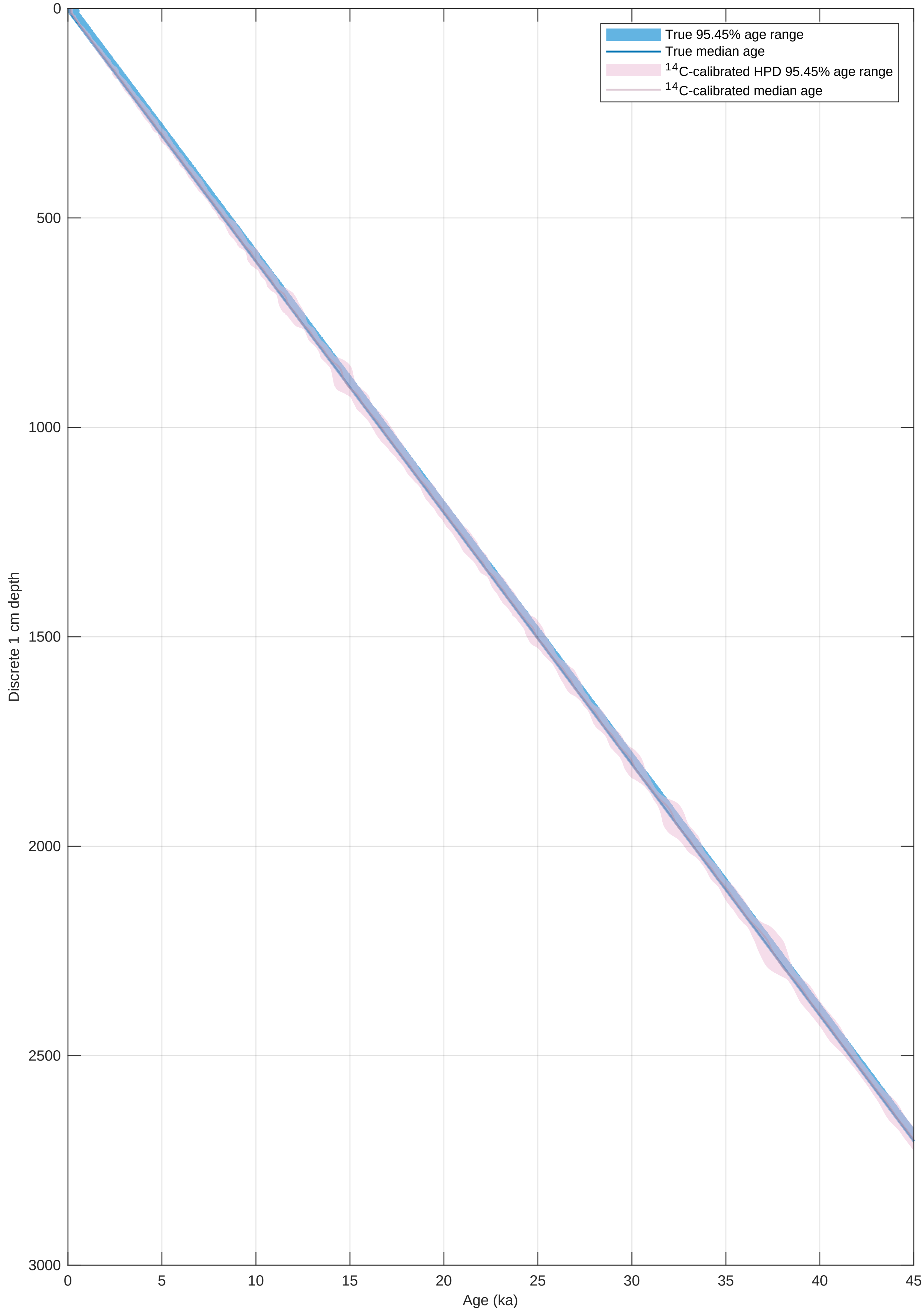

Figure S5. Simulated 1 cm discrete-depth 95.45% true age range (light blue), true median age (dark blue), ^{14}C-calibrated 95.45% HPD age range (light pink) and ^{14}C-calibrated median age (dark pink for whole foraminifera in a simulation scenario with a constant SAR of 60 cm ka-1, constant BD of 10 cm and 0% broken foraminifera.

Constant SAR of 5 cm ka^{-1} with:
constant BD of 10 cm, constant abundance of 100% and 10% broken foraminifera

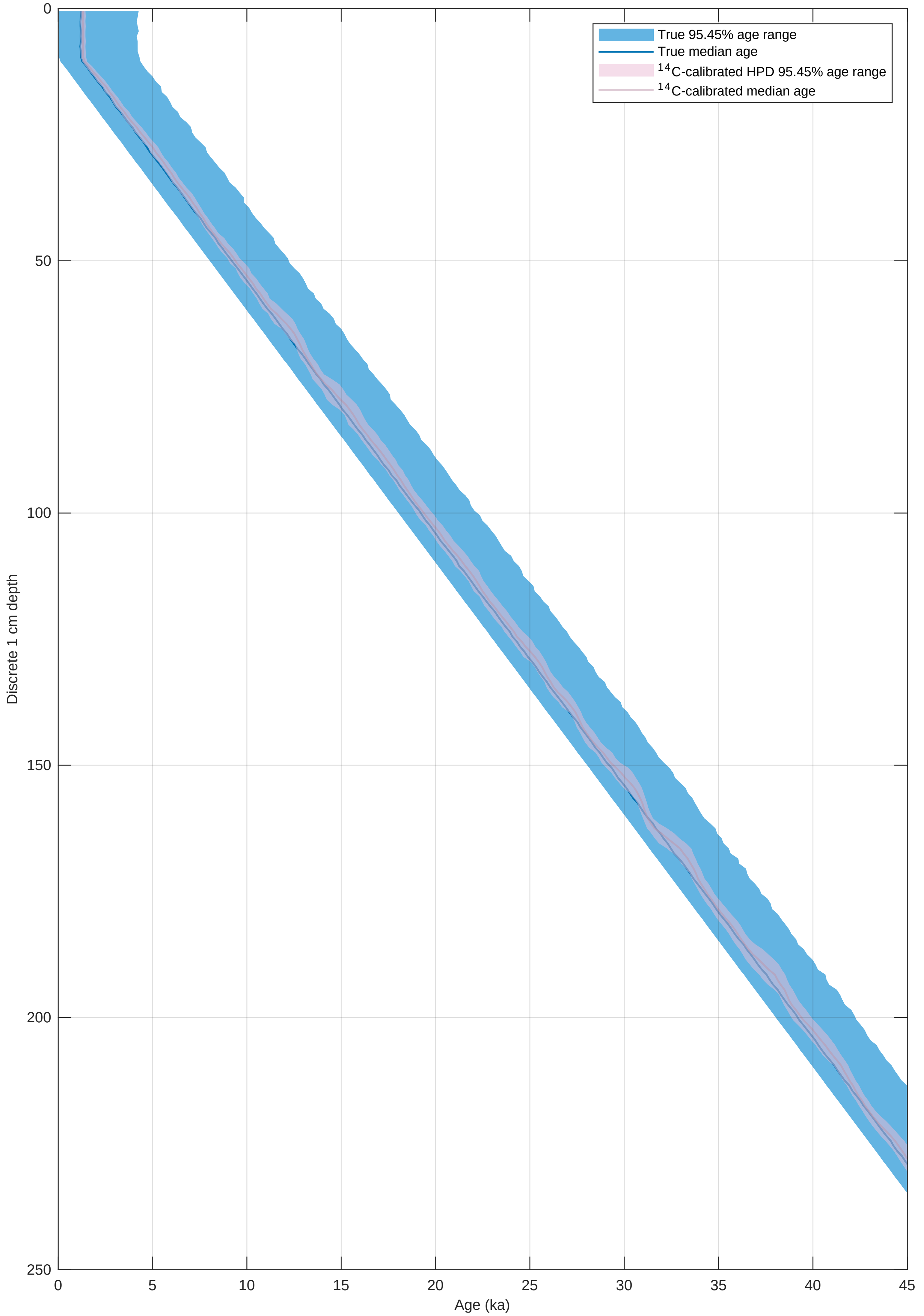

Figure S6. Simulated 1 cm discrete-depth 95.45% true age range (light blue), true median age (dark blue), ^{14}C-calibrated 95.45% HPD age range (light pink) and ^{14}C-calibrated median age (dark pink for whole foraminifera in a simulation scenario with a constant SAR of 5 cm ka-1, constant BD of 10 cm and 10% broken foraminifera.

Constant SAR of 10 cm ka^{-1} with:
constant BD of 10 cm, constant abundance of 100% and 10% broken foraminifera

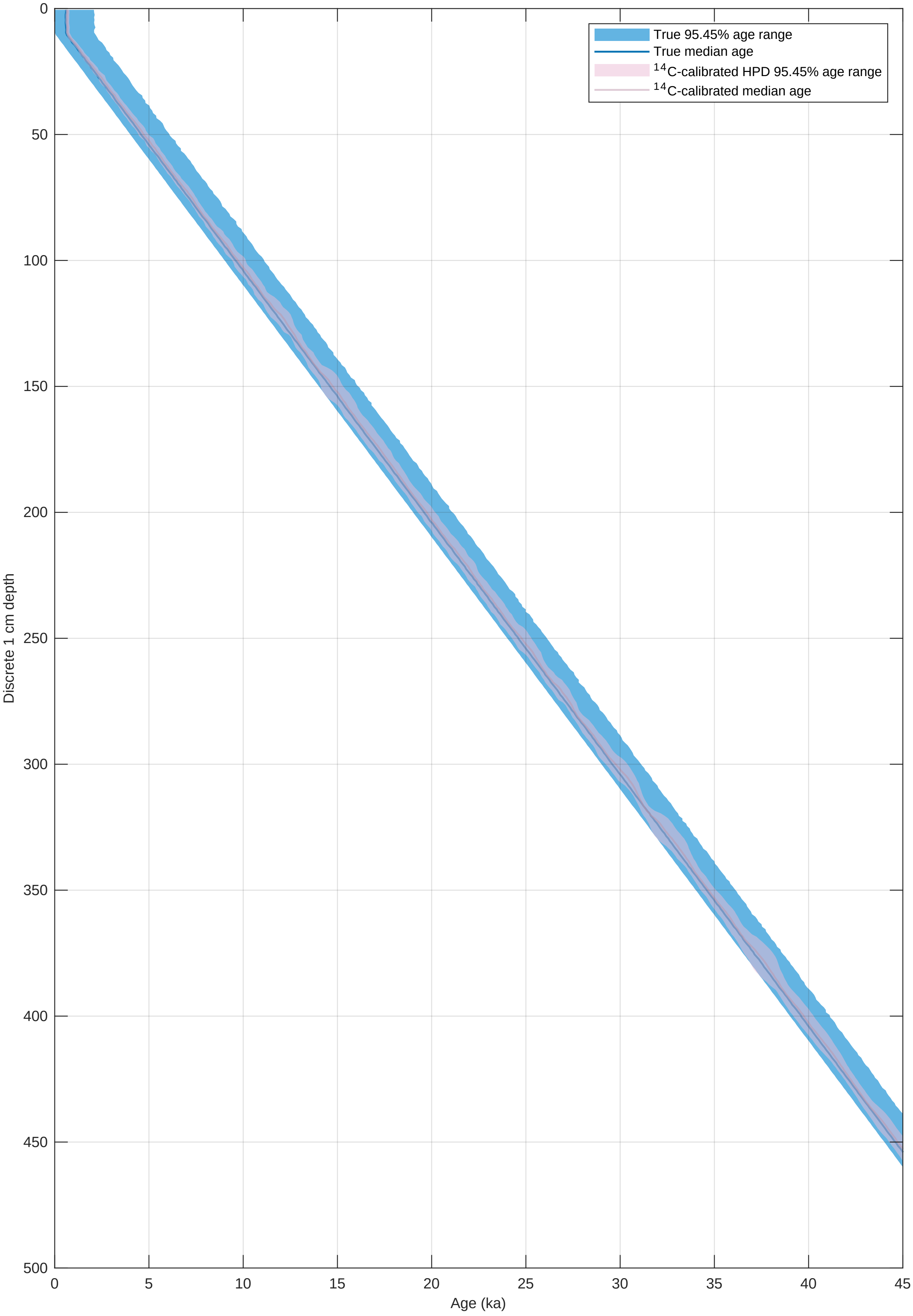

Figure S7. Simulated 1 cm discrete-depth 95.45% true age range (light blue), true median age (dark blue), ^{14}C-calibrated 95.45% HPD age range (light pink) and ^{14}C-calibrated median age (dark pink for whole foraminifera in a simulation scenario with a constant SAR of 10 cm ka-1, constant BD of 10 cm and 10% broken foraminifera.

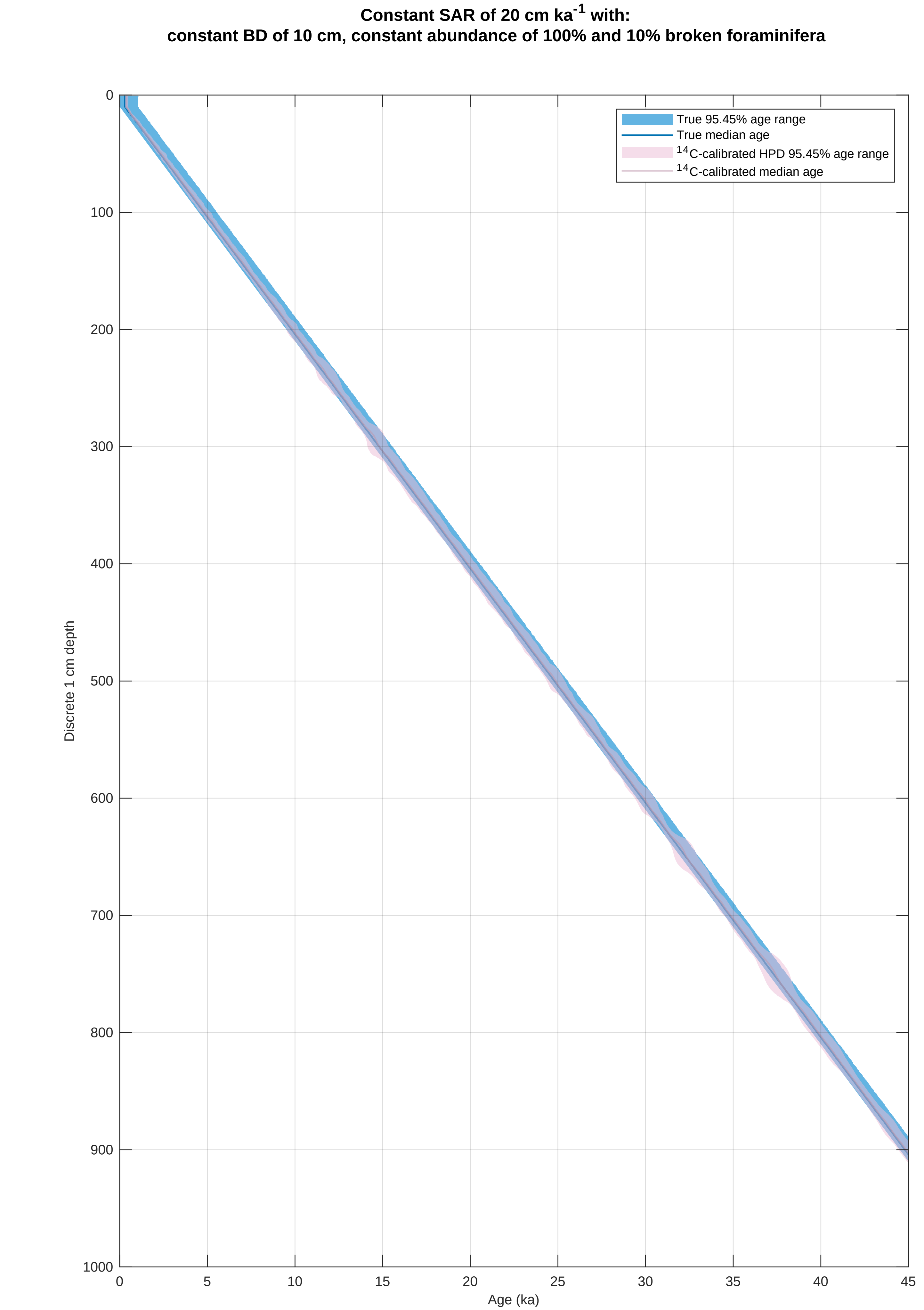
Constant SAR of 20 cm ka^{-1} with:
constant BD of 10 cm, constant abundance of 100% and 10% broken foraminifera
True 95.45% age range
True median age
^{14}C-calibrated HPD 95.45% age range
^{14}C-calibrated median age
Discrete 1 cm depth
Age (ka)
0
100
200
300
400
500
600
700
800
900
1000
0
5
10
15
20
25
30
35
40
45

Figure S8. Simulated 1 cm discrete-depth 95.45% true age range (light blue), true median age (dark blue), ^{14}C-calibrated 95.45% HPD age range (light pink) and ^{14}C-calibrated median age (dark pink for whole foraminifera in a simulation scenario with a constant SAR of 20 cm ka-1, constant BD of 10 cm and 10% broken foraminifera.

Constant SAR of 40 cm ka^{-1} with:
constant BD of 10 cm, constant abundance of 100% and 10% broken foraminifera

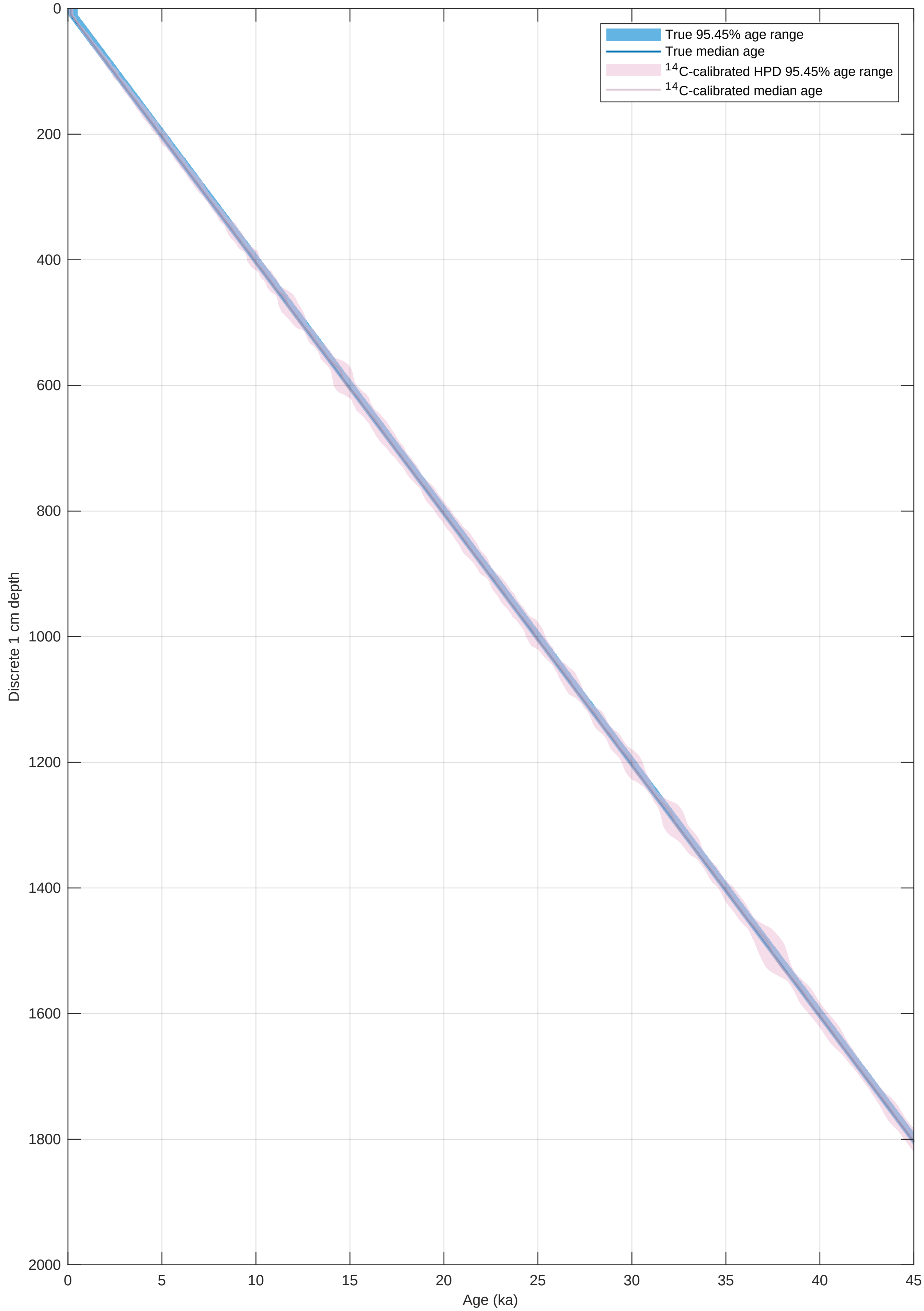

Figure S9. Simulated 1 cm discrete-depth 95.45% true age range (light blue), true median age (dark blue), ^{14}C-calibrated 95.45% HPD age range (light pink) and ^{14}C-calibrated median age (dark pink for whole foraminifera in a simulation with a constant SAR of 40 cm ka-1, constant BD of 10 cm and 10% broken foraminifera.

Constant SAR of 60 cm ka^{-1} with:
constant BD of 10 cm, constant abundance of 100% and 10% broken foraminifera

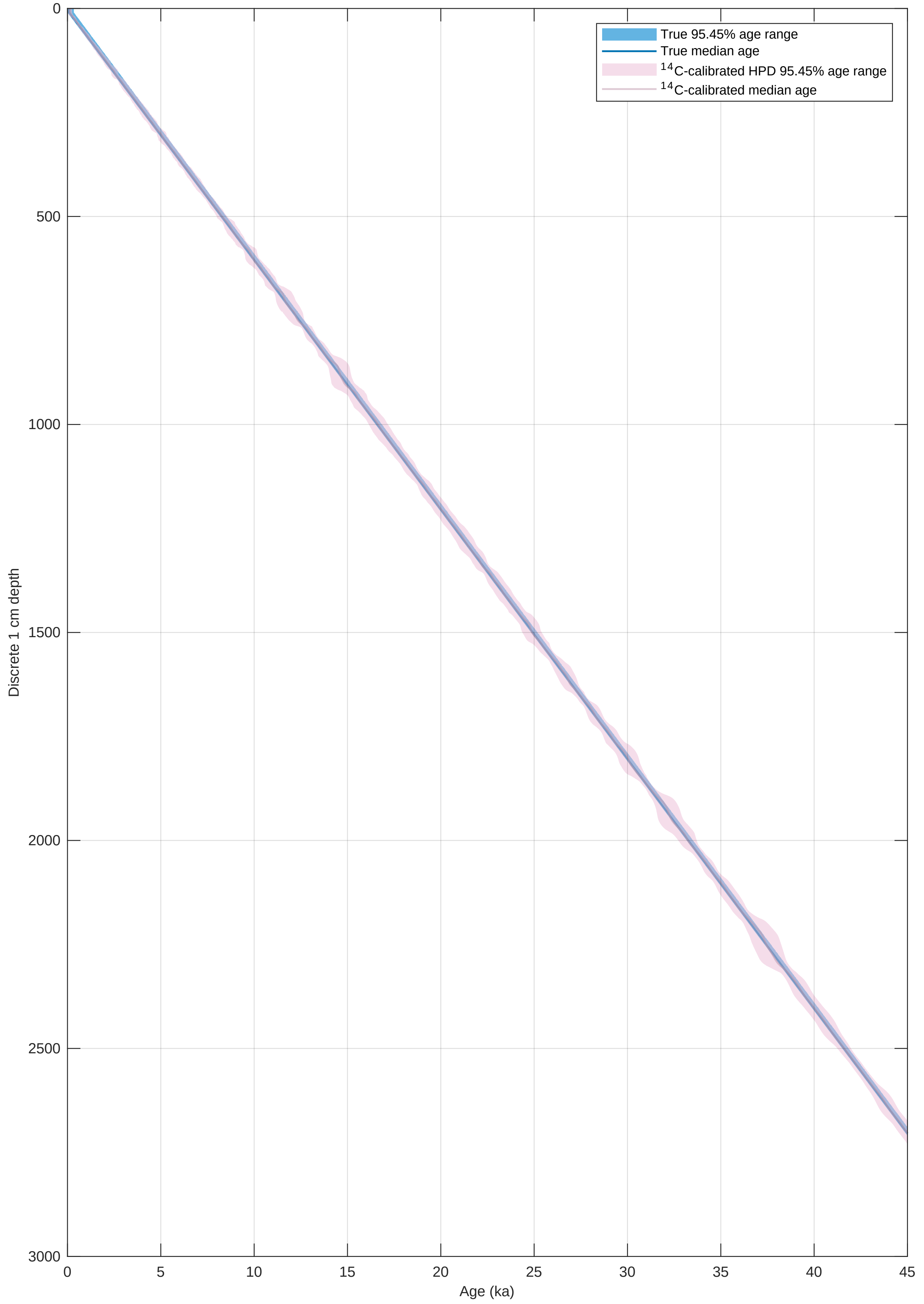

Figure S10. Simulated 1 cm discrete-depth 95.45% true age range (light blue), true median age (dark blue), ^{14}C-calibrated 95.45% HPD age range (light pink) and ^{14}C-calibrated median age (dark pink for whole foraminifera in a simulation scenario with a constant SAR of 60 cm ka-1, constant BD of 10 cm and 10% broken foraminifera.

Simulation output using dynamic input parameters (see Figs. 5a-d) and 10% broken foraminifera

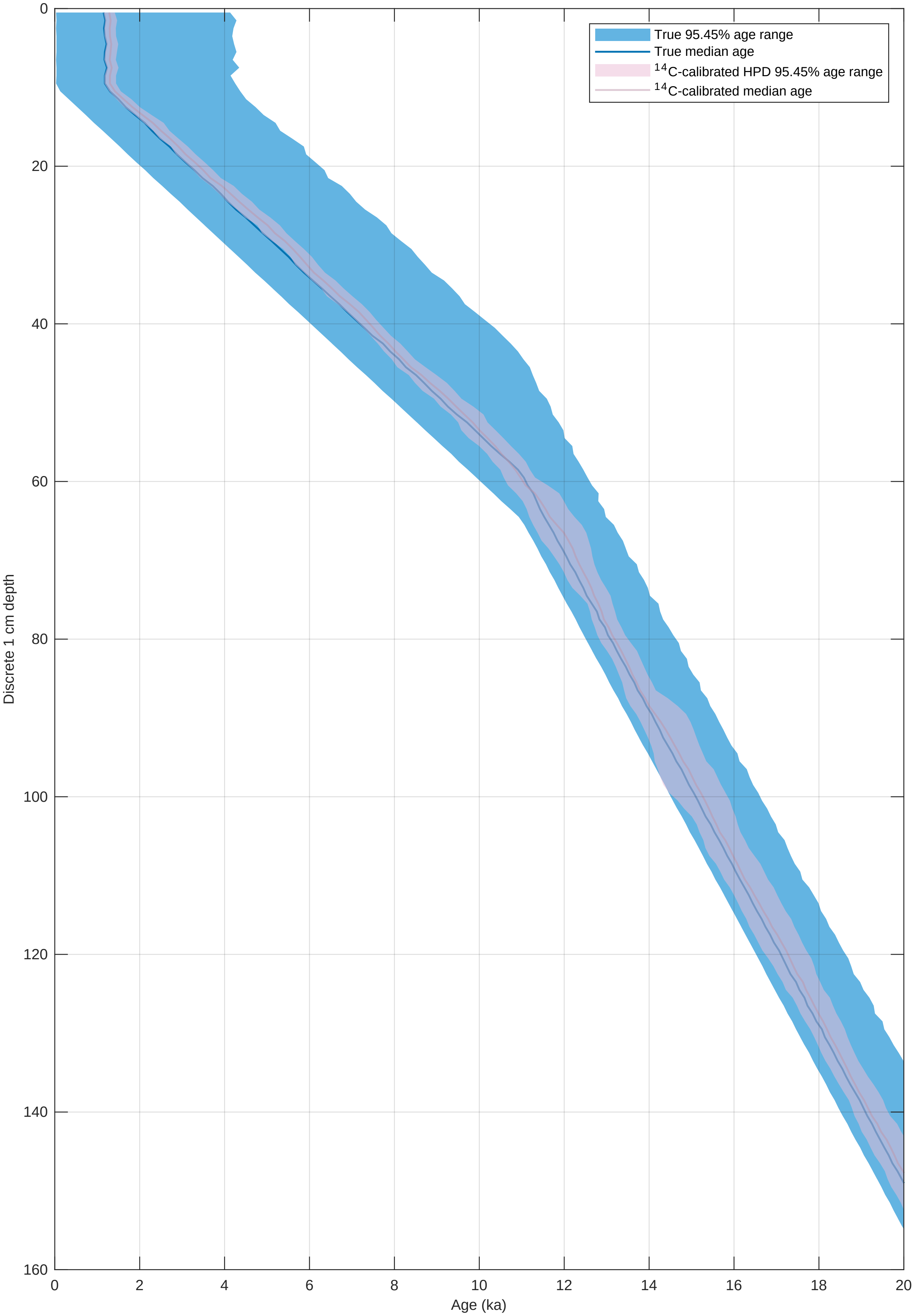

Figure S11. Simulated 1 cm discrete-depth 95.45% true age range (light blue), true median age (dark blue), ^{14}C-calibrated 95.45% HPD age range (light pink) and ^{14}C-calibrated median age (dark pink for whole foraminifera in a simulation scenario using the dynamic inputs detailed in Fig. 5a, 5b, 5c and 5d and 10% broken foraminifera.